AIMS Mathematics, 10(5): 12631–12660.
DOI: 10.3934/math.2025570
Received: 23 December 2024
Revised: 14 March 2025
Accepted: 24 March 2025
Published: 29 May 2025

https://www.aimspress.com/journal/Math

Research article

Bifurcation analysis of a diffuse large b-cell lymphoma growth model in germinal center

Sulasri Suddin[1,2], Fajar Adi-Kusumo[1,*], Mardiah Suci Hardianti[3] and Gunardi[1]

[1] Department of Mathematics, Faculty of Mathematics and Natural Sciences, Universitas Gadjah Mada, Yogyakarta, Indonesia

[2] Universitas Timor, Kefamenanu, Indonesia

[3] Division of Hematology and Medical-Oncology, Department of Internal Medicine, Faculty of Medicine, Public Health and Nursing, Universitas Gadjah Mada, Yogyakarta, Indonesia

* **Correspondence:** Email: f_adikusumo@ugm.ac.id.

Abstract: In this paper, a new mathematical model of diffuse large B-cell lymphoma (DLBCL) in the germinal center and its microenvironment has been considered. The model is a five-dimensional system of first-order nonlinear ordinary differential equations that consists of interactions between centroblasts, centrocyts, plasmablasts, DLBCL cells, and effector cells. Our analysis focuses on understanding the long-term behavior of the DLBCL from a mathematical perspective. The cycle characteristics of DLBCL growth that can be used to detect the duration of the dormant states of the cancer cells and to choose the treatment methods are important to study. By using codimension-one and codimension-two bifurcations, we found Hopf bifurcations that show the appearance of the cycle and some bifurcations of the periodic solutions that are able to be used to characterize the cycle of the disease. In our case, by varying the carrying capacity parameter and the decay rate of effector cells due to the competition with DLBCL, the system undergoes a Hopf bifurcation and then is followed by a generalized Hopf bifurcation, a limit point bifurcation, and a branch point bifurcation. The occurrence of these bifurcations is crucial for understanding the role of effector cells in the regulation of the DLBCL cycle. Furthermore, the appearance of chaotic solutions reflects the irregularity of the system due to changes in initial conditions, highlighting potential uncertainty in the progression of DLBCL metastasis.

Keywords: diffuse large b-cell lymphoma; stability of equilibrium; numerical solution; bifurcation
Mathematics Subject Classification: 34K13, 34K18, 92B05, 92C37

1. Introduction

Cancer is one of the leading causal factors of death worldwide. Based on GLOBOCAN data, there were approximately ten million deaths due to cancer in 2022, see [1]. The cancer cells have the possibility to be treated better into clearance level if they are detected in an earlier stage. It is enabling the timely diagnosis and the treatment of cancer.

Lymphoma is a hematopoietic malignant lymphoid tissue that has similar characteristics to cancer. It accounts for one of ten most common types of human cancer in Australia and the United States [2,3]. There are two general classifications of lymphoma, i.e., Hodgkin lymphoma (HL) and non-Hodgkin lymphoma (NHL). Based on the GLOBOCAN report [1], the new cases of NHL occur almost seven times more than HL, where the number of new invasive NHL cases was estimated at $553,010$ and the deaths were estimated at $250,475$ worldwide. Meanwhile, there were around $80,550$ new cases and $20,180$ deaths of NHL based on the American Cancer Society report in 2023 [3]. In line with other studies, in [4], the authors showed that the number of NHL cases in Indonesia is higher than HL in 2022.

Diffuse large B-cell lymphoma (DLBCL) is the most common and heterogeneous histological subtype of aggressive B-cell NHL. This disease has a diffuse growth pattern and is capable of replacing surrounding normal tissue or organs microscopically. A total 25–40% of adult represent NHL cases reported worldwide [5].

There are three subtypes of DLBCL. The first one is germinal center B-cell (GCB) DLBCL, the second one is activated B-cell (ABC) DLBCL, and the third one is called primary mediastinal B-cell lymphoma, where this type does not express the gene characteristics of GCB or ABC; see [5,6].

The DLBCL can be treated with a standard series of R-CHOP, i.e., *rituximab*, *cyclophosphamide*, *vincristine*, *doxorubicin*, and *prednisone*, where about 60–70% of patients are sustained and they have complete remission, and about 30–40% of patients are relapsed/refractory (R/R), see [7]. Currently, some clinical tools are widely used to predict the overall survival of DLBCL patients; see [8–10]. However, we have not been able to identify the high-risk patients or R/R patients optimally by using those tools [7].

The development of treatment strategies in DLBCL patients is still challenging for health practitioners and professionals. In this paper, we consider the mechanism of DLBCL growth involving centroblasts, centrocyts, plasmablasts, and the effector cells in mathematical perspective. Our study is important to detect the appearance of DLBCL in earlier stages.

In Byrne [11], the authors point out that the collaboration of mathematical and biological models of cancer in the last 50 years accelerated the development of cancer treatment methods and strategies. Several mathematical models have been proposed to study cancer–immune system interactions. For instance, mathematical models focusing on the immune response and its therapeutic implications in tumor invasion have been developed; see [12, 13]. Meanwhile, other models have considered the interaction between cervical cancer and the immune system; see [14–16]. Furthermore, age-structured mathematical models of tumor growth have also been explored to capture more detailed dynamics of cancer progression [17]. Some other mathematical models describe the interactions between tumor or cancer cells, the immune response, and treatment combinations involving chemotherapy and oncolytic viruses; see [18–20]. In addition, models that consider the effects of chemotherapy have also been studied in [21–23].

Studies on stochastic disturbances in tumor dynamics during chemotherapy have been conducted using various approaches. For example, Gaussian white noise affects the stability of the system, where one equilibrium point remains stable only if the noise intensity is weak, while the other equilibrium points remain unstable [24]. In contrast, Gaussian colored noise shows that, in addition to intensity, time correlation also plays a role in system stability. This phenomenon of noise-enhanced stability suggests that stability can be regulated by adjusting time correlation parameters, which has implications for controlling tumor stability during chemotherapy [25]. A tumor-immune model incorporating noise is used to understand the impact of biological uncertainty on chemotherapy efficacy and system stability. In addition to these studies, developing a mathematical model aimed at understanding and predicting the effects of immunotherapy on lymphoma cells has also been explored [26, 27]. A continuous-time Markov process-based model of competition among naïve, normal, and lymphoma T cells has also been proposed [28].

While mathematical modeling has been widely used to study cancer dynamics, models specifically focusing on DLBCL in the germinal center remain limited. Recently, Sabir et al. [29] proposed a mathematical model describing the interaction between CAR T-cells and DLBCL in lymph nodes, providing insights into treatment response and immunosuppression mechanisms. Additionally, Ganesh et al. [30] developed a mathematical model to investigate drug resistance dynamics in DLBCL, exploring interclonal interactions between drug-sensitive and drug-resistant cell populations. However, their study does not explicitly focus on the germinal center microenvironment, which plays a crucial role in lymphoma progression. On the other hand, medical research indicates that the exact cause of DLBCL remains unknown. However, several risk factors have been identified that may increase the likelihood of developing DLBCL [31]. Additionally, studies suggest that DLBCL arises from abnormal mutations of B cells occurring during the differentiation process in the germinal center, initiated by the activation-induced cytidine deaminase (AID) protein [32]. Furthermore, research has shown that DLBCL originates from centroblasts or plasmablasts undergoing abnormal transformations [5, 33].

Our study aims to fill this gap by developing a model that specifically captures the progression of DLBCL within the germinal center, considering B cells as the origin of lymphoma development, particularly centroblasts and plasmablasts. By incorporating key factors influencing disease progression and immune response, our model provides a complementary perspective to existing studies, offering insights into the early-stage dynamics of DLBCL within its microenvironment. Understanding the prognosis of DLBCL at the cellular level in mathematical perspective is a new study. We propose a new model that describes the general behavior of DLBCL without health interventions by considering the interaction between the centroblasts, centrocyts, plasmablasts, DLBCL cells, and effector cells in the lymph nodes. The model is a five-dimensional system of ordinary differential equations with twenty-two dimensions of parameter space.

The cycle characteristics of DLBCL are important to be understood. It can be used not only to detect the dormant state of the disease but also regarding the treatment strategies in the long-term period. From a mathematical point of view, we use codimension-one and codimension-two bifurcations to detect the appearance of Hopf bifurcations and some other bifurcations of the periodic solutions that are important to understand the characteristics of the cycle. In this case, we found Hopf bifurcation that is followed by generalized Hopf bifurcation, limit point bifurcation, and branch point bifurcation for the continuations of the carrying capacity parameter and the decay rate parameter of the effector cells due to the competition with DLBCL.

The paper is organized as follows: In Section 2, we introduce the formulation of the growth of DLBCL in germinal centers as well as the local stability analysis of the steady-state solutions. In Section 3, we perform numerical simulations of the model based on the results of some medical references. Those simulations are important to support and validate the analytical results of the model compared with the medical facts qualitatively. We will close this paper with some concluding remarks.

2. Formulation of DLBCL model

2.1. The origins of DLBCL subtypes derived from germinal center

The germinal center (GC) microenvironment that has a major role in normal B-cell differentiation is the main source of memory and plasma cells that play important roles in the high-affinity antibody production that is needed to protect against microorganisms invasion. However, the beneficial role of GC B cells in immunity is offset by their detrimental role in lymphomagenesis. It is due to the fact that the majority of B-cell lymphomas originate from GC B cells [34].

There are two distinct regions of the GC, i.e., the dark zone (DZ) and the light zone (LZ). The normal process that occurs in the development of GC is as follows. The GC B cells divide and mutate in the DZ and then migrate to the LZ, where they capture antigen via their immunoglobulin surface and present it to the T follicular helper cell [34]. The DZ region consists of centroblasts, which are rapidly proliferating cells that are able to divide every 6–12 hours [35] and then undergo the genes random somatic hypermutations (SHM) that code for immunoglobulin's variable region. After dividing 1–6 times, the centroblasts have the ability to undergo transition to the LZ, where their newly modified B cell receptor (BCR) affinity for antigen is tested. The cells, which are not selected in the LZ or damaged during SHM in the DZ, undergo apoptosis. The LZ consists of non-replicative B cells called centrocytes and presents several types of cells, including follicular dendritic cells (FDC), T follicular helper (TFH), and macrophages [34]. Activation-induced cytidine deaminase (AID), a protein that is necessary for undergoing SHM and for class switch recombination (CSR), is expressed in the GC, particularly in centroblasts, and lower in centrocytes [32].

Next, we provide some biological facts that occur in the early stages of DLBCL growth in the GC on the lymph node. The migration of DZ to LZ is mediated by chemokine receptors $CXCR4$ (LZ-DZ) and $CXCR5$ (DZ-LZ) [33]. The GCB DLBCL cells, which originate from the LZ in the germinal center, displays differentiation towards germinal center B cell characteristics. Conversely, the ABC DLBCL cells arise from early-stage germinal center cells differentiating into plasmablasts, predominantly originating from the DZ [5]. Moreover, plasmablasts that are responsible for antibody production undergo rapid clonal expansion but exhibit a short lifespan [36].

Our study is focused on understand the dynamics of the cells in the tissue near the DLBCL site during the GC reaction, where the behavior of lymphoma is assumed to be homogeneous. The growth of DLBCL that starts from the occurrence of the abnormal centroblasts and the abnormal plasmablasts undergoes abnormal genetic mutations, which are initiated by AID during SHM/CSR.

Based on the ideas of [37, 38], the growth rates of DLBCL cells and centroblasts are assumed to follow the logistic growth. The effector cells that play a role in eliminating the DLBCL cells are CD8+ T cells and natural killer (NK) cells. Those cells are assumed to have positive growth parameters, and their growth follows the Michaelis-Menten reaction; see [37, 39]. Those types of cells are often found in the paracortex of lymph nodes.

The reactions between effector cells and DLBCL cells are able to lead to the inactivation of effector cells or the death of the DLBCL cells. The DLBCL cell has an important role in stimulating the response of the effector cell without an immunoediting mechanism. In the absence of the tumor, the effector cells will undergo apoptosis to maintain homeostasis and to contribute to the generation of memory cells. The ability of the effector cells to eliminate the abnormal cells is not considered in this model. Furthermore, some interactions that occur between centroblasts and plasmablasts with DLBCL cells involve a series of biochemical reactions.

Based on those facts and assumptions, we show the interaction of DLBCL cells with immune cells during the GC reaction in Figure 1.

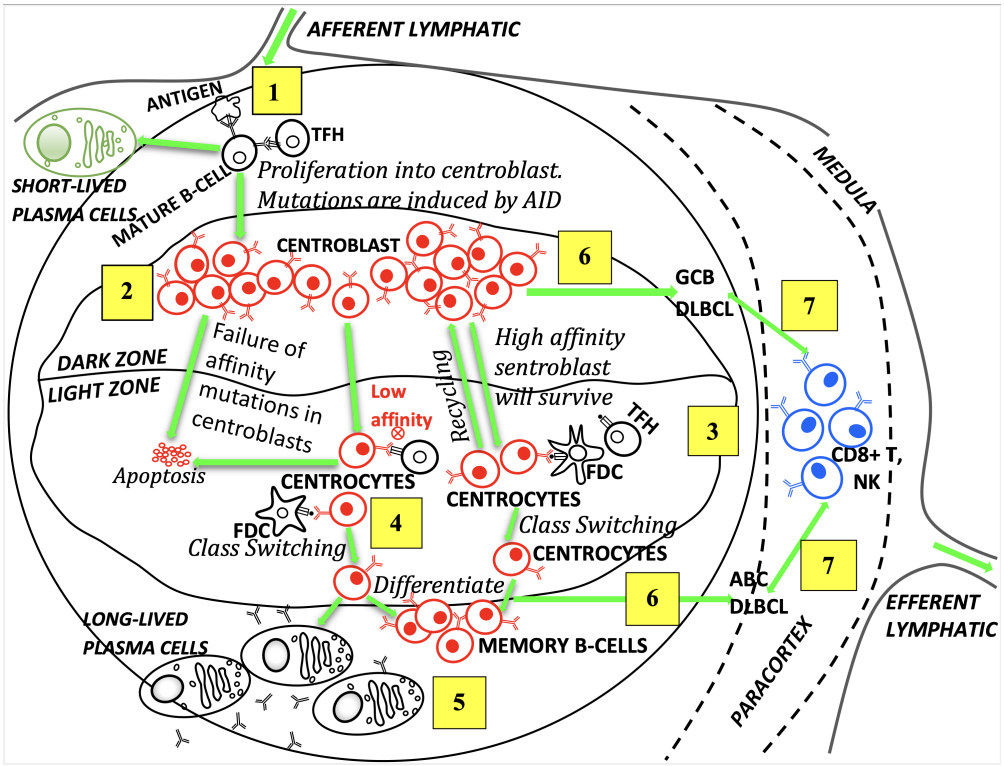

Figure 1. Early growth of DLBCL. (1) Formation of GC through B cell activation; (2) Proliferation and SHM by B cells in the DZ; (3) B cells migrate from the DZ to the LZ; (4) Selection based on affinity for antigen is carried out through interaction with FDC and TFH in the LZ. After positive selection, cells can return to the DZ for mutation or clonal expansion; (5) Selected cells differentiate into plasma cells or memory B cells, while low-affinity cells undergo apoptosis; (6) DLBCL is considered an AID-induced proliferative malignancy; (7) Response of effector cells to the presence of DLBCL.

In this paper, we create a new mathematical model, which is formed as a five-dimensional system of differential equations, where the variables consist of centroblasts (B) and plasmablasts (P) that potentially trigger DLBCL, centrocytes (C), DLBCL cells (T), and effector cells (I). Based on Figure 1, we compose the components of the origins of DLBCL growth in Figure 2.

Figure 2 shows the DLBCL cell progression as a result of abnormal cell division of centroblasts and plasmablasts in the germinal center environment of the lymph node.

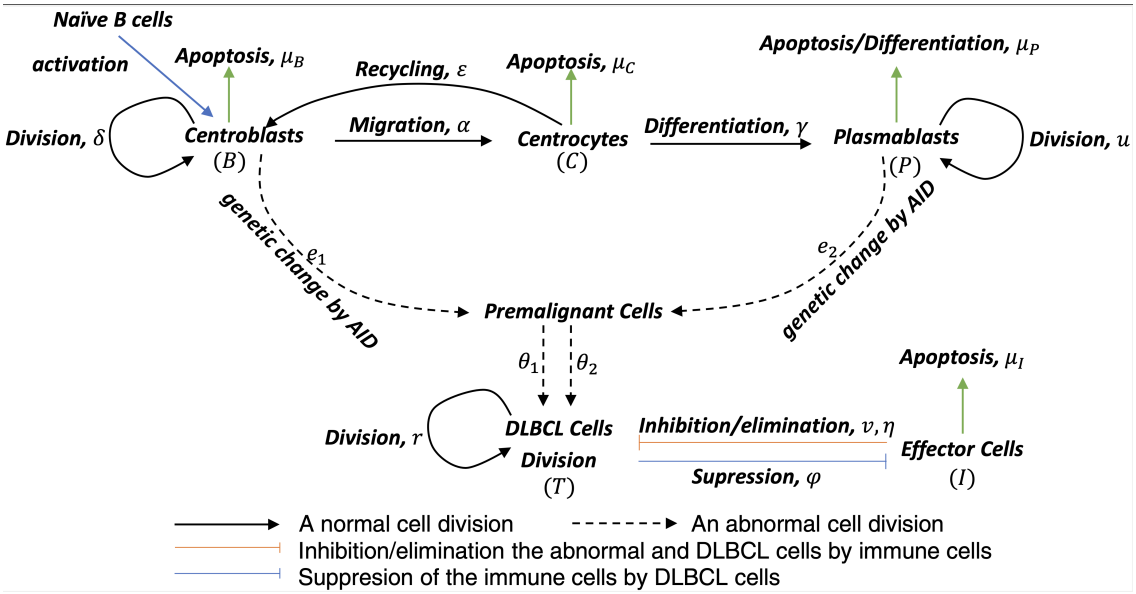

Figure 2. Biological scenarios of DLBCL progression and its interaction with effector cells.

The biological processes of each concentration are described as follows. First, the centroblasts concentration increases with logistic growth rate expressed by the term $\delta\, B\,(1 - bB)$ in the model. The parameter δ represents the centroblast growth rate and $\frac{1}{b}$ shows the carrying capacity of the maximum concentration of centroblasts that can be accommodated in the GC. Logistic growth was chosen for the centroblast concentration because it reflects the limited space and resources in the germinal center. As centroblasts proliferate, the available resources such as nutrients, survival signals, and space within the GC becomes increasingly limited. This leads to apoptosis or differentiation into centrocytes, ensuring that only B cells with high affinity for the antigen survive. The logistic model accurately captures this balance between cell proliferation and regulatory processes within the GC. The recruitment of centroblasts due to the presence of centrocytes with BCR against their specific antigen o that they recirculate to the DZ is denoted by ε. Parameter α denotes the migration of centroblasts to the LZ mediated by the $CXCR5$ signal. Then, centroblasts undergo apoptosis with the rate μ_B and interact with DLBCL cells with decay rate e_1. Therefore,

$$\frac{dB}{dt} = \delta B\,(1 - bB) + \varepsilon C - e_1 BT - (\alpha + \mu_B)\, B.$$

Centrocytes have three potential pathways depending on the affinity of the BCR for antigen [34,35]. The first pathway is the programmed centrocytes' cell apoptosis. It happens when the cells are not able to recognize their specific antigen called not positively selected [34]. This pathway is denoted by μ_C. The second one is the centrocytes whose high-affinity BCRs for the positively selected antigen by TFH cells. It has been rescued from the apoptosis that differentiates into plasmablasts, which is also called pre-plasma cells. It is denoted by γ. Last, centrocytes, which are only capable of interacting with TFH cells, have the ability to evade apoptosis. However, they are not sufficient for positive selection in the LZ, and then undergo recycling to the DZ mediated by $CXCR4$ signals. The rate is denoted by ε.

Additionally, the centrocyte recruitment is an effect of the centroblast migration to the LZ by α,

$$\frac{dC}{dt} = \alpha B - (\varepsilon + \gamma + \mu_C) C.$$

Plasmablast concentrations proliferate with the rate u. Centrocytes that successfully undergo positive selection in the LZ are capable of differentiating into plasmablasts by γ. Then, when DLBCL cells inhibit or attack the plasmablasts with the rate e_2, the plasmablasts also undergo apoptosis with the rate μ_P, if they do not immediately differentiate into plasma cells. As a result, the plasmablast concentrations rate at time t is given by

$$\frac{dP}{dt} = uP + \gamma C - e_2 PT - \mu_P P.$$

The DLBCL cell recruitment is stimulated by two things. First, the abnormal centroblasts and plasmablasts are able to be the DLBCL following the Michaelis-Menten reaction. The maximal conversion rate of abnormal centroblasts is expressed as θ_1, and then the increasing of the total concentration of DLBCL cells follows the Michaelis-Menten term $\frac{\theta_1 BT}{k_1+T}$ where k_1 is the Michaelis-Menten constant that represents the DLBCL cells addition by abnormal centroblasts. Likewise, the maximal conversion rate of abnormal plasmablasts is denoted by θ_2. Furthermore, the total concentration of DLBCL cells can increase with the term $\frac{\theta_2 PT}{k_2+T}$, where k_2 represents the Michaelis-Menten constant for the recruitment of DLBCL cells by abnormal plasmablasts. The recruitment of DLBCL cells by abnormal centroblasts and plasmablasts is modeled using Michaelis-Menten kinetics because it accurately captures the saturation effect observed in enzyme-substrate interactions. In this analogy, abnormal centroblasts and plasmablasts act as enzymes, while DLBCL cells serve as the substrates. At low concentrations of DLBCL cells, the recruitment rate increases as abnormal cells efficiently convert these substrates. However, as DLBCL cell concentration rises, recruitment saturates due to limited resources, reflecting the saturation effect. This non-linear behavior, where the recruitment rate increases initially but slows as the number of available DLBCL cells grows, is well described by the Michaelis-Menten function, making it an ideal choice for modeling this process.

Second, DLBCL cells exhibit intrinsic logistic growth modeled by $rT\,(1 - aT)$, where r denotes the growth rate, and $\frac{1}{a}$ represents the carrying capacity of DLBCL cells in the lymph node. The maximal decay rate of DLBCL cells by those effector cells is given by v. Furthermore, we obtain

$$\frac{dT}{dt} = rT\,(1 - aT) - vTI + \frac{\theta_1 BT}{k_1 + T} + \frac{\theta_2 PT}{k_2 + T}.$$

The recruitment of effector cells is stimulated by cancer antigens produced by DLBCL cells on their surface. The concentration of effector cells will increase following the Michaelis-Menten equation represented by the term $\frac{\eta TI}{k+T}$, where η is the increasing rate of the effector cell, and k is the proliferation rate of the effector cell by DLBCL. In addition, the interaction between effector cells and DLBCL cells can also inhibit the effector cells, where the inhibition rate is φ. The death rate of the Effector cells is denoted by μ_I. For that reason, we obtain

$$\frac{dI}{dt} = \frac{\eta TI}{k + T} - \varphi TI - \mu_I I.$$

By putting all the equations together, the DLBCL growth model in the germinal center can be expressed through a system of ordinary differential equations,

$$\frac{dB}{dt} = \delta B(1-bB) + \varepsilon C - e_1 BT - (\alpha + \mu_B) B, \tag{2.1}$$

$$\frac{dC}{dt} = \alpha B - (\varepsilon + \gamma + \mu_C) C, \tag{2.2}$$

$$\frac{dP}{dt} = uP + \gamma C - e_2 PT - \mu_P P, \tag{2.3}$$

$$\frac{dT}{dt} = rT(1-aT) - vTI + \frac{\theta_1 BT}{k_1 + T} + \frac{\theta_2 PT}{k_2 + T}, \tag{2.4}$$

$$\frac{dI}{dt} = \frac{\eta TI}{k+T} - \varphi TI - \mu_I I, \tag{2.5}$$

where the initial conditions are $B(0) = B_0$, $C(0) = C_0$, $P(0) = P_0$, $T(0) = T_0$, $I(0) = I_0$. Additionally, all variables and parameters in Systems (2.1)–(2.5) are assumed to be non negative.

2.2. Existence of equilibrium points

The DLBCL-free equilibrium is defined as the condition that DLBCL cells do not appear in the lymph node, i.e., $T = 0$ is satisfied. The following theorem gives the guarantees for the existence of equilibrium.

We consider the Systems (2.1)–(2.5). Before presenting the theorem, namely Theorems 2.1–2.3, we define the following set of parameters, which is important to determine the existence of equilibrium points: $\xi_1 = \frac{b\delta}{e_1}$, $\xi_2 = \frac{1}{e_1}\left(\frac{\varepsilon\alpha}{\nu_2} + \delta - \nu_1\right)$, $\nu_1 = \alpha + \mu_B$, $\nu_2 = \varepsilon + \gamma + \mu_C$, $\tilde{\zeta} = \frac{1}{a}$, $\zeta^* = \frac{u-\mu_P}{e_2}$, and $\hat{\zeta} = \frac{(\eta-\mu_I-\varphi k)}{2\varphi} \pm \frac{\sqrt{(\eta-\mu_I-\varphi k)^2 - 4\varphi k\mu_I}}{2\varphi}$. Let $\hat{\zeta}_+ = \frac{(\eta-\mu_I-\varphi k)}{2\varphi} + \frac{\sqrt{(\eta-\mu_I-\varphi k)^2-4\varphi k\mu_I}}{2\varphi}$ and $\hat{\zeta}_- = \frac{(\eta-\mu_I-\varphi k)}{2\varphi} - \frac{\sqrt{(\eta-\mu_I-\varphi k)^2-4\varphi k\mu_I}}{2\varphi}$.

Now, we present the existence conditions for the equilibrium points.

Theorem 2.1. *The equilibrium point $E_0 = [0,\ 0,\ 0,\ 0, 0]$ of the system exists anywhere. The other equilibrium point, i.e., $E_1 = \left[\frac{\xi_2}{\xi_1}, \frac{\alpha\xi_2}{\nu_2\xi_1}, -\frac{\alpha\gamma\xi_2}{\nu_2 e_2 \xi_1 \zeta^*}, 0, 0\right]$, exists for $\xi_2 > 0$ and $\zeta^* < 0$.*

Proof. For $\frac{dT}{dt} = 0$ in Eq (2.4), we have $T = 0$ or $r(1-aT) - vI + \frac{\theta_1 B}{k_1+T} + \frac{\theta_2 P}{k_2+T} = 0$, and for $\frac{dI}{dt} = 0$, we have $I = 0$ or $\frac{\eta T}{k+T} - \varphi T - \mu_I = 0$. Thus, we obtain three cases as a combination of those two conditions while still considering the steady state condition of System (2.1)–(2.5). If $T = 0$ and $I = 0$, by direct calculation, we found that two equilibrium points were obtained, i.e., E_0 as the trivial state where all the populations are zero, and E_1 that exists if $\xi_2 > 0$ and $\zeta^* < 0$. The condition of $\xi_2 > 0$ indicates that centroblasts undergo a transition to the bright zone and differentiate into centrocytes. This process can contribute to lymphoma development if abnormal mutations occur. Meanwhile, $\zeta^* < 0$ indicates that the rate of plasmablast proliferation is lower than the rate of apoptosis. This means that more plasmablasts die than proliferate, leading to a decrease in the plasmablast population, which may contribute to the loss of immune response or impaired antibody production. □

In Theorem 2.1, we have found two equilibrium points with $T = 0$ and $I = 0$. The equilibrium point E_1 with the condition $\zeta^* < 0$, has less possibility to occur in a biological system. Based on [36], it is generally known that the proliferation rate of plasmablasts is higher than their apoptosis rate. However, our existence condition $\zeta^* > 0$ suggests a scenario where the proliferation rate is lower than

the apoptosis rate, which may not be typical but is still possible. This condition does not necessarily invalidate the biological relevance of the $\zeta^* > 0$ case, as it represents a potential but uncommon biological scenario.

Theorem 2.2. *(1) The equilibrium point* $E_2 = \left[0,\ 0,\ 0,\ \widetilde{\zeta}, 0\right]$ *of the system exists for all values of parameters. (2) If* $0 < \widetilde{\zeta} < \zeta^*$*, then the equilibrium point* $E_3 = \left[0, 0, \frac{ra}{\theta_2}\left(\zeta^* - \widetilde{\zeta}\right)(k_2 + \zeta^*), \zeta^*, 0\right]$ *exists. (3) If* $\xi_2 > \widetilde{\zeta} > \zeta^*$*, then exists the other equilibrium point, i.e.,* $E_6 = \left[\kappa P_6, \frac{\alpha}{\nu_2}\kappa P_6, P_6, \frac{1}{e_1}\left(\delta\left(1 - b\kappa P_6\right) + \frac{\varepsilon\alpha}{\nu_2} - \nu_1\right), 0\right]$ *where* $\kappa = \left(\frac{\xi_2 - \zeta^*}{\frac{\alpha\gamma}{e_2\nu_2} + \xi_1 P_6}\right)$ *by considering* $k_1 + \zeta^* = k_2 + \zeta^* = 0$*. Furthermore, if* E_6 *satisfies*

(1) $r_0 > \frac{q_0^2}{3}$*, then* P_6 *takes the form*

$$P_6 = \sqrt[3]{\frac{-b_0}{2} + \sqrt{\frac{b_0^2}{4} + \frac{a_0^3}{27}}} - \sqrt[3]{\frac{b_0}{2} + \sqrt{\frac{b_0^2}{4} + \frac{a_0^3}{27}}} - \frac{q_0}{3},$$

or

(2) $r_0 < \frac{q_0^2}{3}$*, then* P_6 *takes the form*

$$P_6 = \sqrt{-\frac{a_0}{3}}\cos(\frac{\psi}{3}) - \frac{q_0}{3},$$

where $a_0 = \frac{1}{3}\left(3r_0 - q_0^2\right)$, $b_0 = \frac{1}{27}\left(2q_0^3 - 9q_0r_0 + 27s_0\right)$, $\cos\psi = -\sqrt{\frac{b_0^2}{4}/\frac{a_0^3}{-27}}$, $r_0 = \frac{\alpha\gamma}{\theta_2 e_2^2 \nu_2 \xi_1^2}\left(\left(rae_2\xi_1\left(\widetilde{\zeta} - \zeta^*\right) + \theta_1 e_2\right)(\xi_2 - \zeta^*) + \frac{\theta_2\alpha\gamma}{\nu_2}\right)$,
$q_0 = \frac{1}{\theta_2 e_2 \xi_1}\left(\theta_1 e_2\left(\xi_2 - \zeta^*\right) + \frac{2\theta_2\alpha\gamma}{\nu_2}\right)$, *and* $s_0 = \frac{ra\alpha^2\gamma^2}{\theta_2 e_2^2 \nu_2^2 \xi_1^2}\left(\widetilde{\zeta} - \xi_2\right)(\xi_2 - \zeta^*)$.

Proof. For $r(1 - aT) - vI + \frac{\theta_1 B}{k_1 + T} + \frac{\theta_2 P}{k_2 + T} = 0$ and $I = 0$, by solving $\frac{dB}{dt} = \frac{dC}{dt} = 0$, we get $B = 0$ and $T = -\xi_1 B + \xi_2$. Then, we have two equilibrium points, i.e., E_2 that exists anywhere and E_3 that exists for $0 < \widetilde{\zeta} < \zeta^*$. Now, for $T = -\xi_1 B + \xi_2$, $\frac{dC}{dt} = \frac{dP}{dt} = 0$, and $r(1 - aT) - vI + \frac{\theta_1 B}{k_1 + T} + \frac{\theta_2 P}{k_2 + T} = 0$, we get $4th$-degree polynomial equation and can be written as

$$z_0 P^4 + z_1 P^3 + z_2 P^2 + z_3 P + z_4 = 0, \tag{2.6}$$

where

$$\begin{aligned}
z_0 &= \theta_2 e_2^3 \xi_1^3 (k_1 + \zeta^*), \\
z_1 &= {e_2}^2 \xi_1^2 (rae_2\xi_1\left(\widetilde{\zeta} - \zeta^*\right)(k_1 + \zeta^*)(k_2 + \zeta^*) + \theta_1 e_2(\xi_2 - \zeta^*)(k_2 + \zeta^*) + \\
&\quad \frac{\theta_2\alpha\gamma}{\nu_2}(3k_1 + \xi_2 + 2\zeta^*)), \\
z_2 &= e_2\frac{\alpha\gamma}{\nu_2}\xi_1(rae_2\xi_1(\left(\left(\widetilde{\zeta} - \xi_2\right)(k_1 + \zeta^*) + (k_1 + \xi_2)\left(\widetilde{\zeta} - \zeta^*\right)\right)(k_2 + \zeta^*) + \\
&\quad \left(\widetilde{\zeta} - \zeta^*\right)(k_1 + \zeta^*)(k_2 + \xi_2)) + \theta_1 e_2(\xi_2 - \zeta^*)(2k_2 + \xi_2 + \zeta^*) + \\
&\quad \frac{\theta_2\alpha\gamma}{\nu_2}(3k_1 + 2\xi_2 + \zeta^*)),
\end{aligned}$$

$$z_3 = \frac{\alpha^2\gamma^2}{\nu_2^2}(rae_2\xi_1((\widetilde{\zeta}-\xi_2)(k_1+\xi_2)(k_2+\zeta^*)+((\widetilde{\zeta}-\xi_2)(k_1+\zeta^*)+ (\widetilde{\zeta}-\zeta^*)(k_1+\xi_2))(k_2+\xi_2))+e_2\theta_1(k_2+\xi_2)(\xi_2-\zeta^*)+\theta_2\frac{\alpha\gamma}{\nu_2}(k_1+\xi_2)),$$

$$z_4 = ra\frac{\alpha^3\gamma^3}{\nu_2^3}(\widetilde{\zeta}-\xi_2)(k_1+\xi_2)(k_2+\xi_2),$$

by considering $\tilde{\zeta} = \frac{1}{a}$ and $\zeta^* = \frac{u-\mu_P}{e_2}$. Let $k_1+\zeta^* = k_2+\zeta^* = 0$, then (2.6) becomes a cubic polynomial, i.e.,

$$P^3 + q_0P^2 + r_0P + s_0 = 0, \tag{2.7}$$

where $q_0 = \frac{1}{\theta_2e_2\xi_1}\left(\theta_1e_2(\xi_2-\zeta^*)+\frac{2\theta_2\alpha\gamma}{\nu_2}\right)$, $s_0 = \frac{ra\alpha^2\gamma^2}{\theta_2e_2^2\nu_2^2\xi_1^2}(\widetilde{\zeta}-\xi_2)(\xi_2-\zeta^*)$, and $r_0 = \frac{\alpha\gamma}{\theta_2e_2^2\nu_2\xi_1^2}\left(\left(rae_2\xi_1(\widetilde{\zeta}-\zeta^*)+\theta_1e_2\right)(\xi_2-\zeta^*)+\frac{\theta_2\alpha\gamma}{\nu_2}\right)$, satisfies $\xi_2 > \widetilde{\zeta} > \zeta^*$. Obviously, $q_0, r_0 > 0$, $s_0 < 0$, and $r_0 > q_0$. This condition indicates that (2.7) has exactly one positive real root based on Descartes' rule of signs. Equation (2.7) can be reduced by substitution

$$P = w - \frac{q_0}{3} \tag{2.8}$$

into the normal form

$$w^3 + a_0w + b_0 = 0, \tag{2.9}$$

where $a_0 = \frac{1}{3}\left(3r_0-q_0^2\right)$ and $b_0 = \frac{1}{27}\left(2q_0^3-9q_0r_0+27s_0\right)$. If $r_0 > \frac{q_0^2}{3} > 0$ then $a_0 > 0$ and $b_0 < 0$ are obtained. In addition, Polynomials (2.9) have exactly one positive root provided $b_0 < 0$ and $\frac{b_0^2}{4}+\frac{a_0^3}{27} > 0$, $w = A - B$, where

$$A = \sqrt[3]{-\frac{b_0}{2}+\sqrt{\frac{b_0^2}{4}+\frac{a_0^3}{27}}}, B = \sqrt[3]{\frac{b_0}{2}+\sqrt{\frac{b_0^2}{4}+\frac{a_0^3}{27}}}. \tag{2.10}$$

It is clear that $A > B > 0$ thus results in $w > 0$. From Eq (2.8), we have the positive root of a Polynomial (2.7), P_6. Meanwhile, if $0 < r_0 < \frac{q_0^2}{3}$ then $a_0 < 0$ and $b_0 > 0$. Noted $\frac{b_0^2}{4}+\frac{a_0^3}{27} < 0$. Since $b_0 > 0$ and according to [40], Polynomial (2.9) has two positive roots, w_i and w_j, of the form

$$w_i = 2\sqrt{-\frac{a_0}{3}}\cos\left(\frac{\psi}{3}\right), w_j = 2\sqrt{-\frac{a_0}{3}}\cos\left(\frac{\psi+4\pi}{3}\right), \tag{2.11}$$

where $\cos\psi = -\sqrt{\frac{b_0^2}{4}/\frac{a_0^3}{-27}}$. Each of w_i and w_j corresponds to a root of a Polynomial (2.7) of the form (2.8). We get $-1 \le \cos\psi < 0$ or $\frac{\pi}{2} < \psi \le \pi$ so that $\cos\left(\frac{\psi}{3}\right) \ge \cos\left(\frac{\psi+4\pi}{3}\right)$. This shows that $w_i \ge w_j$. Because $w_i \ge w_j$ and it is known that the Polynomial (2.7) has exactly one positive root, the positive real root that satisfies is w_i, so (2.8) becomes $P_6 = w_i - \frac{q_0}{3}$. Thus, it can be concluded that for Case 2 ($\delta(1-bB) - e_1T + \frac{\varepsilon\alpha}{\nu_2} - \nu_1 = 0$) which $k_1+\zeta^* = k_2+\zeta^* = 0$, then a Polynomial (2.6) has exactly one positive root as long as it satisfies $\xi_2 > \widetilde{\zeta}$, $\xi_2 > \zeta^*$, and if it satisfies the conditions: $r_0 > \frac{q_0^2}{3}$ or $r_0 < \frac{q_0^2}{3}$. Simultaneously it is proven that E_6 exists. □

The condition $k_1+\zeta^* = k_2+\zeta^* = 0$ at the equilibrium point E_6 signifies that the growth of plasmablast concentration is influenced by the proliferation and decay of centroblasts, either through apoptosis or abnormal mutations, in proportion to the concentration of DLBCL cells required by enzymes in centroblasts or plasmablasts to attain maximum reaction rates. Then, in Theorem 2.2, we have found three equilibrium points that $T \neq 0$ and $I = 0$.

Theorem 2.3. *If* $0 < \hat{\zeta} < \widetilde{\zeta}$, *then exists the equilibrium point* $E_4 = \left[0, 0, 0, \hat{\zeta}, \frac{ra}{v}\left(\widetilde{\zeta} - \hat{\zeta}\right)\right]$. *If* $0 < \hat{\zeta} < \xi_2$ *and* $\zeta^* < \hat{\zeta} < \widetilde{\zeta}$, *then we have the equilibrium point* $E_5 = \left[B_5, \frac{\alpha}{\nu_2}B_5, \frac{\alpha\gamma B_5}{e_2\nu_2\left(\hat{\zeta}-\zeta^*\right)}, \hat{\zeta}, \frac{1}{v}\left(ra\left(\widetilde{\zeta} - \hat{\zeta}\right) + B_5\left(\frac{\theta_1}{k_1+\hat{\zeta}} + \frac{\alpha\gamma\theta_2}{e_2\nu_2\left(k_2+\hat{\zeta}\right)\left(\hat{\zeta}-\zeta^*\right)}\right)\right)\right]$. *In addition, for both equilibrium points* E_4 *and* E_5, $\hat{\zeta} > 0$ *must satisfy the following conditions to ensure their existence: (i) The condition* $\eta - \mu_I - \varphi k > 0$ *must hold; (ii) The discriminant condition* $(\eta - \mu_I - \varphi k)^2 \geq 4\varphi k\mu_I$ *must be satisfied to guarantee that* $\hat{\zeta}$ *is real and positive.*

Proof. The condition $\hat{\zeta} > 0$ is satisfied as long as $\eta - \mu_I - \varphi k > 0$ and $(\eta - \mu_I - \varphi k)^2 \geq 4\varphi k\mu_I$. By direct calculation and considering the steady state of the system, the equilibrium point E_4 exists if $0 < \hat{\zeta} < \widetilde{\zeta}$. Furthermore, we also have the other equilibrium point, $E_5 = \left(B_5, C_5, P_5, \hat{\zeta}, I_5\right)$, where $B_5 = \frac{1}{\xi_1}\left(\xi_2 - \hat{\zeta}\right)$, which exists if $0 < \hat{\zeta} < \xi_2$ and $\zeta^* < \hat{\zeta} < \widetilde{\zeta}$. □

In Theorem 2.3, we have found two pairs of equilibrium points, $T = \hat{\zeta}$ and $I \neq 0$. The two pairs of equilibria are E_{4+} and E_{4-}, as well as E_{5+} and E_{5-}. The presence of the ± sign in the solution indicates two distinct values for T, leading to two corresponding equilibrium points. We obtain two equilibrium points: E_{4+} and E_{4-} for the first pair, and E_{5+} and E_{5-} for the second pair. These pairs of equilibrium points are determined under the given conditions of the system and correspond to the positive roots of $T = \hat{\zeta}$. Specifically, the equilibrium point E_4 is biologically relevant and exists when the carrying capacity of the DLBCL cells is greater than the concentration of effector cells, along with a concurrent reduction in the number of effector cells. This suggests that in the context of DLBCL dynamics, the conditions for E_4 represent a feasible scenario where lymphoma growth is restrained due to the imbalance between the lymphoma cell carrying capacity and effector cell concentration. On the other hand, the equilibrium point E_5 represents a scenario where all cell populations have survived the competition and coexist harmoniously. In other words, the DLBCL cells persist, but their concentration is sufficiently low compared to the different cell types. This indicates a balanced state where the immune system, particularly the effector cells, can effectively control the DLBCL population, leading to a stable coexistence with a low lymphoma burden.

2.3. Stability analysis of equilibrium points

For all values of the parameters, the stability of the equilibrium points is described by the following theorems.

Theorem 2.4. *The equilibrium points* E_0 *and* E_1 *are saddle-types.*

Proof. By using linear analysis, we found that near equilibrium point E_0, there are five eigenvalues i.e., $-\mu_I$, r, $\frac{-(\nu_1+\nu_2-\delta)\pm\sqrt{\left((\nu_1+\nu_2-\delta)^2-4(\nu_2(\nu_1-\delta)-\varepsilon\alpha)\right)}}{2}$, $u - \mu_P$, and $-\nu_1$. Thus, E_0 is unstable (saddle-type). By the same manner, we have the eigenvalues of the equilibrium point E_1, are $-\mu_I$, $r + \frac{\theta_1}{b\delta k_1}\left(\frac{\varepsilon\alpha}{\nu_2} + \delta - \nu_1\right) +$

$\frac{\alpha\gamma\theta_2}{b\delta\mu_P k_2\nu_2}\left(\frac{\varepsilon\alpha}{\nu_2}+\delta-\nu_1\right)$ (always positive based on the existence condition of equilibrium point E_1), $u-\mu_P$, $-\nu_2$, and $\delta-2\left(\delta+\frac{\varepsilon\alpha}{\nu_2}-\nu_1\right)-\nu_1$. Thus, E_1 is also unstable (saddle-type). □

The trivial equilibrium point E_0 is interpreted as the absence of all cell populations. It indicates the extinction of cells or no living cell.

To facilitate the analysis in Theorems 2.5 and 2.6 on the stability of equilibrium points, we introduce the following parameters: $\Gamma_1 = \frac{\eta\widetilde{\zeta}}{k+\widetilde{\zeta}} - \varphi\widetilde{\zeta} - \mu_I$, $\Gamma_2 = \frac{\eta\zeta^*}{k+\zeta^*} - \varphi\zeta^* - \mu_I$, $\Gamma_3 = \frac{\delta-\left(e_1\widetilde{\zeta}+\nu_1+\nu_2\right)\pm\sqrt{\left(\delta-\left(e_1\widetilde{\zeta}+\nu_1+\nu_2\right)\right)^2-4\left(\left(e_1\widetilde{\zeta}+\nu_1-\delta\right)\nu_2-\varepsilon\alpha\right)}}{2}$, $\Psi_1 = \frac{\delta-\left(e_1\hat{\zeta}+\nu_1+\nu_2\right)\pm\sqrt{\left(\delta-\left(e_1\hat{\zeta}+\nu_1+\nu_2\right),\right)^2-4\left(\left(e_1\hat{\zeta}+\nu_1-\delta\right)\nu_2-\varepsilon\alpha\right)}}{2}$, and $\Psi_2 = \frac{-ra\hat{\zeta}}{2}\pm\frac{1}{2}\sqrt{\left(ra\hat{\zeta}\right)^2-4ra\hat{\zeta}\left(\widetilde{\zeta}-\hat{\zeta}\right)\left(\frac{\eta k}{\left(k+\hat{\zeta}\right)^2}-\varphi\right)}$.

Theorem 2.5. *(1) The equilibrium point E_2 has eigenvalues Γ_1, $-r$, $e_2\left(\zeta^*-\widetilde{\zeta}\right)$, and Γ_3. It is locally asymptotically stable if $\zeta^*<\widetilde{\zeta}$, $\widetilde{\zeta}>\xi_2$, and $\Gamma_1<0$. (2) The equilibrium point E_3 has eigenvalues $\frac{1}{2}\frac{ra\zeta^*}{k_2+\zeta^*}\left(\widetilde{\zeta}-k_2-2\zeta^*\right)\pm\frac{1}{2}\sqrt{\left(\frac{ra\zeta^*}{k_2+\zeta^*}\left(\widetilde{\zeta}-k_2-2\zeta^*\right)\right)^2-4rae_2\zeta^*\left(\zeta^*-\widetilde{\zeta}\right)}$, Γ_2, Γ_3, and it is locally asymptotically stable if $\widetilde{\zeta}>\xi_2$ and $\Gamma_2<0$. Both E_2 and E_3 are unstable (saddle-type) if their eigenvalues are real, have opposite signs, and none are zero.*

Proof. The eigenvalues associated with the equilibrium point E_2, are Γ_1, $-r$, $e_2\left(\zeta^*-\widetilde{\zeta}\right)$, and Γ_3. In order for the eigenvalues of Γ_3 to have all negative real parts, then $\delta-\left(e_1\widetilde{\zeta}+\nu_1+\nu_2\right)<0$ and $\left(e_1\widetilde{\zeta}+\nu_1-\delta\right)\nu_2-\varepsilon\alpha>0$. Both of these conditions occur provided that $\widetilde{\zeta}>\frac{1}{e_1}\left(\frac{\varepsilon\alpha}{\nu_2}+\delta-\nu_1\right)=\xi_2$. The equilibrium point E_2 is locally asymptotically stable for $\zeta^*<\widetilde{\zeta}$, $\widetilde{\zeta}>\xi_2$, and $\Gamma_1<0$. The eigenvalues for equilibrium point E_3, are $\frac{1}{2}\frac{ra\zeta^*}{k_2+\zeta^*}\left(\widetilde{\zeta}-k_2-2\zeta^*\right)\pm\frac{1}{2}\sqrt{\left(\frac{ra\zeta^*}{k_2+\zeta^*}\left(\widetilde{\zeta}-k_2-2\zeta^*\right)\right)^2-4rae_2\zeta^*\left(\zeta^*-\widetilde{\zeta}\right)}$, Γ_2, Γ_3. The equilibrium point E_3 is locally asymptotically stable for $\widetilde{\zeta}>\xi_2$ and $\Gamma_2<0$. Both E_2 and E_3 are unstable (saddle-type) if at least one eigenvalue is positive and at least one is negative, with the condition that none of the eigenvalues are zero. □

The equilibrium point E_2 represents the DLBCL threshold of invasion that indicates the maximum abnormal mutations of the centroblast and plasmablast cells. The stability condition of E_2 is reached when the interaction between DLBCL cells reaches maximum capacity with the contribution of abnormal centroblasts to the appearance of DLBCL cells is larger than the combination between the growth of the normal centroblast and normal plasmablast contributions, supported by continuously decreasing immune cell proliferation. It indicates that the equilibrium point E_2 tends to appear in the GCB subtype (originating from abnormal centroblasts), which is less aggressive compared to the ABC subtype.

By using the same terms, we have the existence of E_3 for $0<\widetilde{\zeta}<\zeta^*$. Those existence conditions imply the limitations of the carrying capacity against DLBCL by the growing concentration of plasmablasts, which are the host that supports the growth of ABC DLBCL, see [5] for the detail. Meanwhile, plasmablast growth is influenced by two important processes, i.e., cell proliferation and decay, as well as other factors such as DNA mutations and apoptosis. An abnormal mutation causes plasmablasts to develop into DLBCL cells before they have time to differentiate into plasma cells. As a result, DLBCL cells gain the ability to invade other healthy plasmablasts.

The threshold of the substances represented by equilibrium point E_3 is reached when the interaction between the carrying capacity of DLBCL and the conversion rate of abnormal centroblasts into DLBCL cells exceed the growth contribution of centroblasts that are in line with the decay of effector cell proliferation.

We note that the stability conditions of E_2 affect the existence of E_3. The equilibrium E_3 only exists when E_2 is unstable, and it disappears when E_2 is asymptotically stable. The situation indicates that the patient is not able to have both ABC DLBCL and GCB DLBCL simultaneously. In general, the composite lymphoma cases are very rare to find; see [41].

Theorem 2.6. *(1) The equilibrium point E_{4-} has eigenvalues $\frac{1}{e_2}\left(\zeta^* - \hat{\zeta}\right)$, Ψ_1, and Ψ_2. It is locally asymptotically stable provided that $\hat{\zeta}_- > \xi_2$, $\zeta^* < \hat{\zeta}_-$, and $(\eta - \mu_I - \varphi k)^2 > 4\varphi k\mu_I$. Then, E_{4-} is unstable (saddle-type) if its eigenvalues are real, have opposite signs, and none are zero. (2) The equilibrium point E_{4+} is unstable (saddle-type) if $\left(\zeta^* - \hat{\zeta}\right) \neq 0$, and Ψ_1 is a real nonzero.*

Proof. Eigenvalues for E_4 are $\frac{1}{e_2}\left(\zeta^* - \hat{\zeta}\right)$, Ψ_1, and Ψ_2. It is clear that $\Psi_1 < 0$ if $\hat{\zeta} > \xi_2$. Consider $\frac{\eta k}{\left(k+\hat{\zeta}\right)^2} - \varphi$ with the existence condition of E_4. If $(\eta - \mu_I - \varphi k)^2 > 4\varphi k\mu_I$, we obtain $\frac{\eta k}{\left(k+\hat{\zeta}_-\right)^2} - \varphi > 0$ such that Ψ_2 having negative real parts or negative values. Simultaneously, we acquire $\frac{\eta k}{\left(k+\hat{\zeta}_+\right)^2} - \varphi < 0$ resulting in Ψ_2 having both negative and positive values. Meanwhile, for $(\eta - \mu_I - \varphi k)^2 = 4\varphi k\mu_I$, we obtain $\frac{\eta k}{\left(k+\hat{\zeta}\right)^2} - \varphi = 0$ such that Ψ_2 having nonpositive values. It is clear that $\frac{\eta k}{\left(k+\hat{\zeta}\right)^2} > \varphi$ is absolutely only fulfilled by $\hat{\zeta}_-$. Hence, the equilibrium point E_{4-} is locally asymptotically stable provided that $\hat{\zeta}_- > \xi_2$, $\zeta^* < \hat{\zeta}_-$, $(\eta - \mu_I - \varphi k)^2 > 4\varphi k\mu_I$, and unstable (saddle-type) when it has at least one positive and one negative eigenvalue, with none equal to zero. Otherwise, E_{4+} becomes unstable due to $\frac{\eta k}{\left(k+\hat{\zeta}_+\right)^2} < \varphi$, saddle-type. Otherwise, E_{4+} becomes unstable due to $\frac{\eta k}{\left(k+\hat{\zeta}_+\right)^2} < \varphi$, and it is a saddle provided that $\frac{1}{e_2}\left(\zeta^* - \hat{\zeta}\right)$ is nonzero, with Ψ_1 being real and nonzero. Moreover, $E_4 = E_{4-} = E_{4+}$ is a non-hyperbolic point due to $\frac{\eta k}{\left(k+\hat{\zeta}_+\right)^2} = \varphi$. □

The equilibrium point E_4 as total DLBCL invasion indicates the presence of resistance. This condition occurs when the carrying capacity of DLBCL cells exceeds the concentration of effector cells, accompanied by a decay in effector cell concentration. Despite the absence of host cells, DLBCL cells and effector cells persist. The recovery of normal cells does not occur due to competition with DLBCL cells, resulting in the elimination of normal cells. In other words, the abnormal cells transform into DLBCL cells, leading to invasion and subsequent metastasis beyond the lymph node tissue.

The equilibrium points E_5 and E_6 are determined through numerical simulations using their bifurcation boundaries in the next section. The equilibrium point E_5 indicates a state in which all cell populations have survived the competition and coexist. While E_6 exists when the growth in centroblast concentration is above the carrying capacity of DLBCL cells and also exceeds the growth in plasmablast concentration.

3. Numerical bifurcation analysis

In this section, we explain some numerical continuation of the equilibrium points to determine some scenarios regarding the stability conditions of the equilibrium points. The analysis is done by using

a numerical continuation toolbox, Matcont, see [42]. The numerical continuation of the equilibrium points of System (2.1)–(2.5) is used to obtain some bifurcations for various parameter sets.

Some parameter values, i.e., u, e_1, e_2, θ_1, and θ_2, are assumed based on relevant biological references. The value of u represents the proliferation of plasmablasts, which arises from the proliferation of antigen-specific B cells and their differentiation during the first six days of the immune response, with plasmablast differentiation occurring between days 3 and 6 [43]. The value of the inactivation rate of centroblasts and plasmablasts, e_1 and e_2, by DLBCL is based on the idea of the inactivation rate of effector cells, such as CD8+ T cells, NK cells, CD4+ T cells, and other hunter cells, by tumors, which ranges from 10^{-12} $cell^{-1}day^{-1}$ to 10^{-6} $cell^{-1}day^{-1}$ [39, 44]. Meanwhile, the maximal conversion rate of abnormal centroblasts and abnormal plasmablasts to DLBCL, denoted as θ_1 and θ_2, is based on the general mutation rate of tumor cells [45].

The details of parameters are also presented in Table 1.

Table 1. Parameter values used for the numerical simulation of System (2.1)–(2.5).

Parameter	Range	Reference
δ	$2.5 - 3\ day^{-1}$	[38, 46]
b	$6.67 \times 10^{-4} cells^{-1}$	[38]
ε	$2.5\ day^{-1}$	[38]
μ_B	$0.3\ day^{-1}$	[38, 46]
α	$0.3 - 2.5\ day^{-1}$	[38, 46]
μ_C	$1.44 - 3.84\ day^{-1}$	[47]
γ	$3.42\ day^{-1}$	[48]
μ_P	$0.2 - 0.33\ day^{-1}$	[36]
r	$0.18 - 0.514\ day^{-1}$	[39, 44]
a	$1.02 \times 10^{-9} - 2.0 \times 10^{-9} cells^{-1}$	[39, 44]
v	$1.101 \times 10^{-7} - 3.23 \times 10^{-7}\ cell^{-1}day^{-1}$	[39, 44]
k_1	$10^5\ cell$	[37]
k_2	$10^5\ cell$	[37]
η	$0.1245\ day^{-1}$	[39]
k	$2.019 \times 10^7 cells$	[39]
φ	$3.422 \times 10^{-10}\ cell^{-1}day^{-1}$	[39]
μ_I	$0.02 - 0.0412\ day^{-1}$	[39]
u	$0.2\ day^{-1}$	Assumed
e_1	$1 \times 10^{-6}\ cell^{-1}day^{-1}$	Assumed
e_2	$1 \times 10^{-6}\ cell^{-1}day^{-1}$	Assumed
θ_1	$1 \times 10^{-2}\ day^{-1}$	Assumed
θ_2	$1 \times 10^{-10}\ day^{-1}$	Assumed

In this case, we consider a codimension two bifurcation analysis of the equilibrium points based on the parameters a and φ that represent the carrying capacity of the DLBCL's concentration and the decay rate of the effector cells as the effects of the interaction with DLBCL, respectively. Those parameters are important because the combination of these two parameters allows for the exploration of stability transitions, particularly between uncontrolled lymphoma growth and other states. This is

crucial for studying the tumor microenvironment's response to biological changes and understanding how cancer weakens the immune system. Such insights are relevant for exploring immune dynamics and the effectiveness of the immune response against cancer.

The details of the bifurcation boundaries are outlined in Table 2.

Table 2. Conditions for the existence and local stability of the equilibrium.

Eq.	Existence conditions	Stability conditions
E_0	-	Unstable
E_1	$\xi_2 > 0 > \zeta^*$	Unstable
E_2	-	Stable if $\zeta^* < \widetilde{\zeta}, \widetilde{\zeta} > \xi_2, \Gamma_1 < 0$
E_3	$0 < \widetilde{\zeta} < \zeta^*$	Stable if $\widetilde{\zeta} > \xi_2, \Gamma_2 < 0$
E_{4+}	$0 < \hat{\zeta}_+ < \widetilde{\zeta}, \eta - \mu_I - \varphi k > 0,$ $(\eta - \mu_I - \varphi k)^2 \geq 4\varphi k\mu_I$	Unstable
E_{4-}	$0 < \hat{\zeta}_- < \widetilde{\zeta}, \eta - \mu_I - \varphi k > 0,$ $(\eta - \mu_I - \varphi k)^2 \geq 4\varphi k\mu_I$	Stable if $\xi_2 < \hat{\zeta}_-, \zeta^* < \hat{\zeta}_-,$ $\eta - \mu_I - \varphi k > 0, (\eta - \mu_I - \varphi k)^2 > 4\varphi k\mu_I$
E_{5_+}	$0 < \hat{\zeta}_+ < \xi_2, \zeta^* < \hat{\zeta}_+ < \widetilde{\zeta},$ $\eta - \mu_I - \varphi k > 0, (\eta - \mu_I - \varphi k)^2 \geq 4\varphi k\mu_I$	Stable/Unstable
E_{5_-}	$0 < \hat{\zeta}_- < \xi_2, \zeta^* < \hat{\zeta}_- < \widetilde{\zeta},$ $\eta - \mu_I - \varphi k > 0, (\eta - \mu_I - \varphi k)^2 \geq 4\varphi k\mu_I$	Stable/Unstable
E_6	$k_1 + \zeta^* = k_2 + \zeta^* = 0, \xi_2 > \widetilde{\zeta} > \zeta^*,$ $\frac{\widetilde{\zeta}-\zeta^*}{\xi_2-\widetilde{\zeta}} > \frac{k_2+\zeta^*}{k_2+\xi_2} + \frac{k_1+\zeta^*}{k_1+\xi_2}$	Stable/Unstable

Eq."Equilibrium".

Based on the existence and stability conditions in Table 2, and by considering the parameter values in Table 1, we obtain set of functions of a and φ. From the condition E_2 we get $a > -1 \times 10^{-4}$, $a < 5.049740484 \times 10^{-7}$, and $\varphi > a\left(\frac{2}{a(1000+\frac{1}{a})} - 0.02\right)$. Based on the conditions of E_3, we obtain $a < -1 \times 10^{-5}$, $a < 5.049740484 \times 10^{-7}$, and $\varphi < -0.2000202020 \times 10^{-4}$. In general, the existence condition for E_4 and E_5 must satisfy $1.98 - 1000\varphi > 0$ and $(1.98 - 1000\varphi)^2 \geq 80\varphi$. The bifurcation boundaries for the existence and stability conditions of E_4 and E_5 are derived based on algebraic computations (see Appendix A for details). For the final one, we acquire the existence of E_6, that is, $-1 \times 10^5 < \frac{1}{a} < 1.980299786 \times 10^6$. In this paper, we consider the bifurcation value with the positive value of a and φ, so that the bifurcation boundary is also considered to be positive, which is relevant to the biological interpretation and behavior of the system.

The diagram below illustrates a codimension two bifurcation for parameters a and φ, along with a zoomed-in view of two specific areas that reveals seven regions with distinct qualitative properties, see Figure 3.

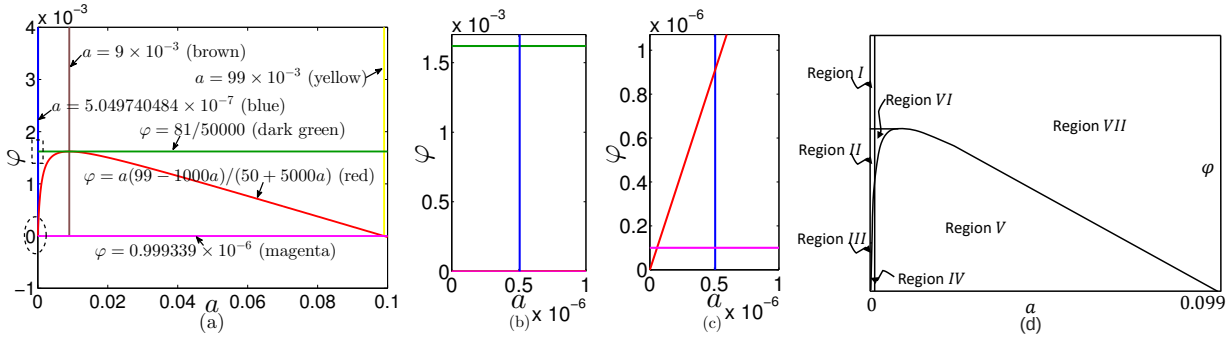

Figure 3. (a) Codimension two bifurcation diagrams that show the continuation of a and φ. The bifurcation boundary that ilustrates some bifurcation scenario of a and φ in the parameter space (a-φ) are represented by: $a = 5.049740484 \times 10^{-7}$ (blue), $a = 9 \times 10^{-3}$ (brown), $a = 99 \times 10^{-3}$ (yellow), $\varphi = 0.999339 \times 10^{-6}$ (magenta), $\varphi = \frac{81}{50000}$ (dark green), and $\varphi = a\left(\frac{2}{1+1000a} - 0.02\right)$ (red). These curves are derived from the existence and stability conditions of equilibrium points, obtained by substituting parameter values from Table 1. The detailed derivation can be found in the previous discussion. (b) Enlarged dashed rectangular detail from Figure (a). (c) Enlarged dashed circle detail from Figure (a). (d) A recaptured result based on Figures (a) to (c), seven regions with different qualitative properties are shown.

Some numerical simulations of the projection of phase portrait and trajectories of the system are presented in Figures 4–13.

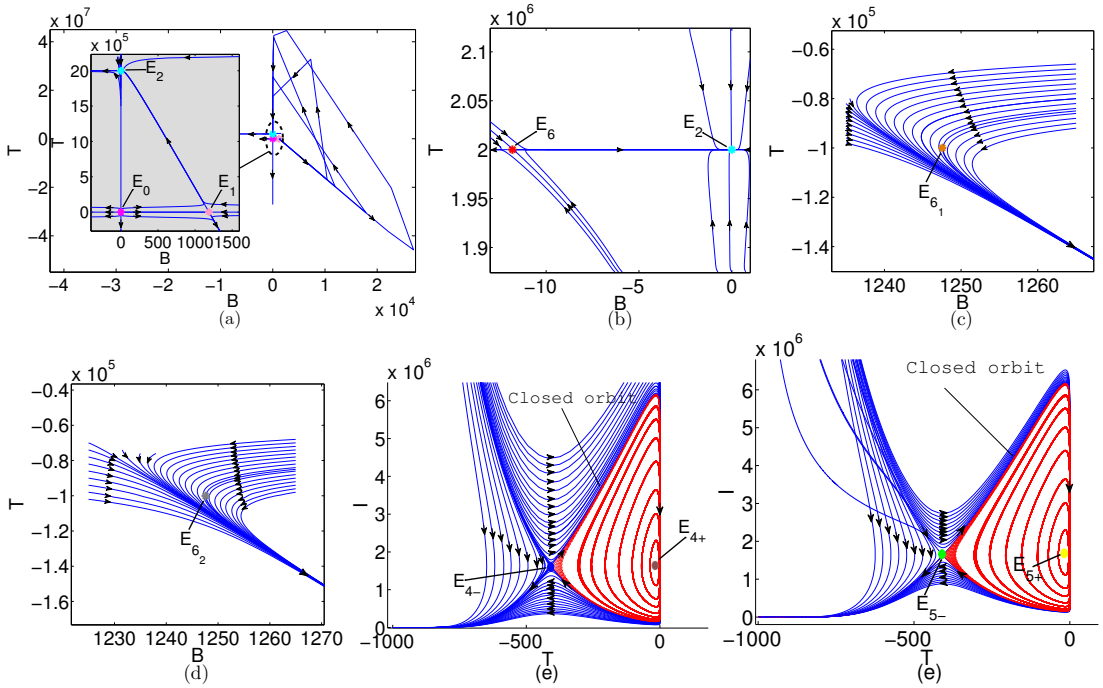

Figure 4. Projection of phase portrait of asymptotically stable and unstable equilibrium points in region I with $a = 5 \times 10^{-7}$ and $\varphi = 3.422 \times 10^{-3}$: E_0-magenta, E_1-pink, E_2-cyan, E_6-red, E_{6_1}-orange, E_{6_2}-grey.

In Figure 4, we show the appearance of several solution behaviors. (a) shows three equilibrium points i.e., two DLBCL-free points E_0 and E_1 which are both saddles, and one equilibrium point E_2 which is locally asymptotically stable. The heteroclinic orbit connects two points, E_0 and E_2, then E_1 and E_2. (b) shows the heteroclinic orbit connecting the saddle point (E_6) and the node point (E_2). (c,d) show that if some initial values are taken around the equilibrium points E_{61} and E_{62}, respectively, the corresponding solutions move away from their respective equilibrium points, indicating instability. No periodic orbits or connections between orbits are visible in this plot. The other equilibrium points are non-hyperbolic (E_{4+}-brown, E_{5+}-yellow) and saddle (E_{4-}-blue, E_{5-}-green) presented in (e,f). There are homoclinic orbits connected by saddle points E_{4-} (e) and E_{5-} (f).

Figure 5: The three subplots (a)–(c) discuss the solution around the equilibrium point E_{4-} with different focuses. Subplot (a) illustrates the final trajectory as a torus that becomes increasingly dense over time. This is supported by the Lyapunov exponents in subplot (b), where four exponents are negative and one is positive, confirming the presence of chaotic oscillations. Subplot (c) presents the phase portrait of (T, I), showing a spiral trajectory that initially moves away from the initial conditions and eventually leads to dense periodic oscillations as $t \to \infty$. This behavior is further reflected in subplot (d), which illustrates the time evolution of $T(t)$, where the increasingly dense oscillations can be directly observed. This pattern indicates a transition to chaotic oscillations, as observed in subplot (a). The continuous fluctuations between DLBCL cells and effector cells during DLBCL growth are likely caused by the interaction dynamics within the tumor microenvironment, where DLBCL cells grow, evade detection, and resist damage by effector cells. In contrast, the concentration of normal cells (centroblasts, centrocytes, and plasmablasts) tends to approach zero, suggesting that the presence of normal cells does not influence the fluctuations between DLBCL cells and effector cells. Subplot (d) demonstrates locally asymptotic stable behavior around $E_{5-} = (1187.577483, 38.14488703, 1304.368175, 14.33344256, 1.635950007 \times 10^6)$, providing insights into the stable coexistence of lymphoma cells, immune cells, and normal cells. When initial conditions are taken near E_{5-}, all trajectories converge toward this equilibrium point, indicating its local asymptotic stability. The presence of DLBCL cells at this equilibrium indicates that lymphoma is not completely eradicated by the immune system. However, its population remains controlled, preventing the destruction of normal or immune cells. Numerical simulations suggest this stability, although an analytical determination of the stability conditions is still an open problem and will be explored in future work.

In Figure 5(b), the chaotic phenomenon indicated by the Lyapunov exponent (E_{4-}) results suggests that DLBCL lymphoma patients with identical initial conditions can exhibit significantly different therapeutic responses or prognostic outcomes. The sensitivity of this model corresponds to the fact that DLBCL is a subtype with high heterogeneity, which can confer different prognoses [5, 6]. This heterogeneity can refer to diversity in genetics, phenotype, and interactions with the immune system. Therefore, it is crucial to identify the most influential parameters in DLBCL development to manipulate the system's more stable or regular behavior. While, Figure 5(d) demonstrates the coexistence of normal cells, DLBCL cells, and effector cells over an extended period. Generally, strategies for both conditions focus on managing DLBCL by maintaining the lymphoma population at a low, controlled level that does not compromise the patient's bodily functions, thereby improving quality of life and clinical outcomes.

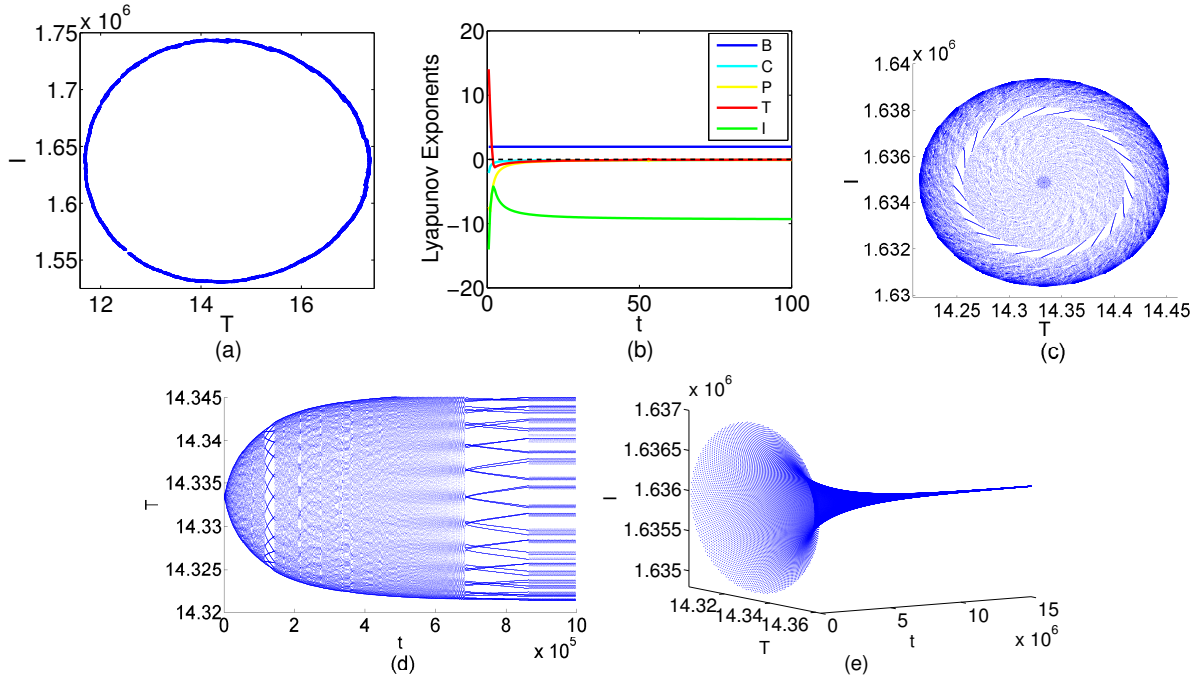

Figure 5. Projection of phase portrait-trajectory near equilibria E_{4-} and E_{5-} in region II. From left to right and top to bottom: (a) cross-section of trajectory over a specific time interval near E_{4-}, (b) dynamic of the Lyapunov exponent near E_{4-}, (c) phase portrait $(T - I)$ near E_{4-}, (d) trajectory $(T - t)$ near E_{4-}, (e) trajectory in phase space $(T - I - t)$ near E_{5-}.

In Figure 6, we show that the DLBCL lymphoma remains in the population at its carrying capacity or moves toward a locally asymptotically stable equilibrium point, E_2. Similarly, selecting initial conditions near E_{5+} also leads the solution toward E_2. Simultaneously, the concentration of normal cells tends towards zero. To reword, DLBCL can "hide" from effector cells to maintain their growth.

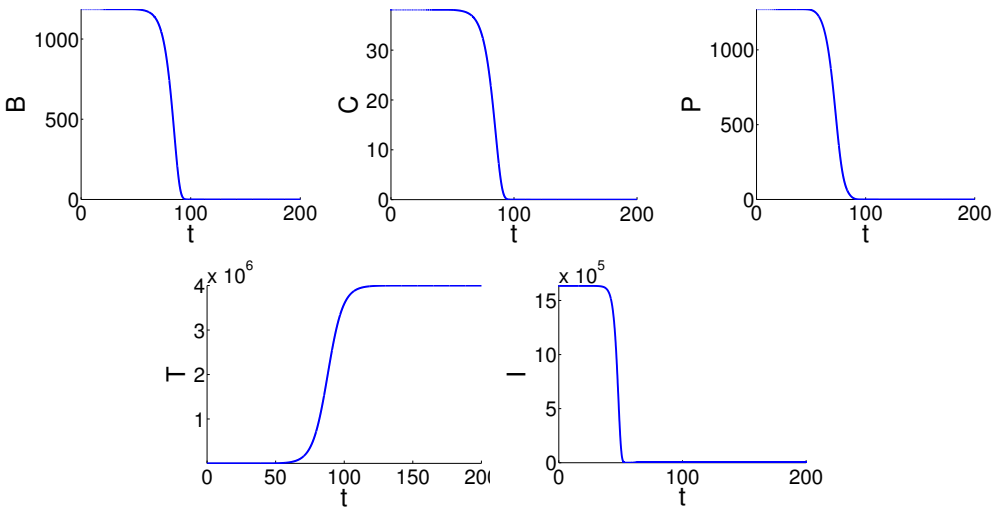

Figure 6. The concentration evolution at E_{5+} in region II.

In Figure 7, the continuation of the equilibrium point E_{4-} leads to a Hopf bifurcation at negative a. However, continuation at the Hopf point with respect to its period yields some LPCs and PDs, which are observed at positive a values. Biologically, only positive a values are relevant, representing the dynamic balance between effector and DLBCL cells. While the Hopf bifurcation initially occurs at a non-biological parameter value ($a < 0$), its continuation reveals sustained oscillations, including LPC2, LPC5, and PD4, which are relevant for understanding the system's long-term dynamics in a biologically meaningful regime.

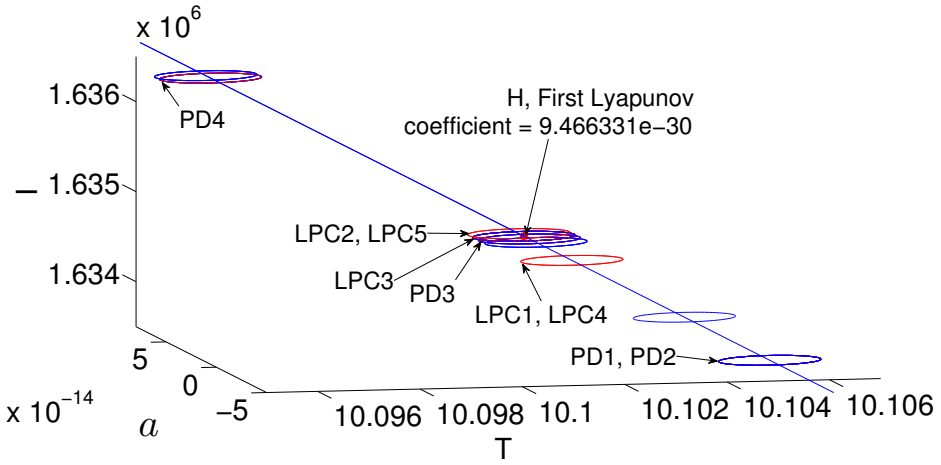

Figure 7. Continuation starting from the non-hyperbolic equilibrium $E_{4-} = (0, 0, 0, 10.10101087, 1.634877384 \times 10^6)$ in region III reveals a Hopf bifurcation as the parameter a varies, with the bifurcation occurring at $a = -2.3196609 \times 10^{-18}$, approaching zero. There is no biological interpretation for this phenomenon, as it occurs when a is negative. Continuation from the Hopf point with respect to the period leads to the emergence of Limit Point Cycle (LPC) and period doubling (PD). All LPCs and PDs share the same period of 1.052473×10^2, with the following corresponding values for a and Normal form coefficients, i.e., LPC1, $a = -2.299093 \times 10^{-18}$, Normal form coefficient = 3.289885×10^{-8}; PD1, $a = -2.448590 \times 10^{-13}$, Normal form coefficient = 1.886291×10^{-18}; PD2, $a = -2.448590 \times 10^{-13}$, Normal form coefficient = 1.940624×10^{-18}; LPC2, $a = 5.274856 \times 10^{-15}$, Normal form coefficient = -1.792046×10^{-8}; LPC3, $a = -3.430147 \times 10^{-18}$, Normal form coefficient = -5.104872×10^{-9}; PD3, $a = -5.395832 \times 10^{-15}$, Normal form coefficient = 6.241529×10^{-15}; LPC4, $a = -4.772857 \times 10^{-14}$, Normal form coefficient = 1.874483×10^{-8}; LPC5, $a = 1.051630 \times 10^{-17}$, Normal form coefficient = -3.799681×10^{-6}; PD4, $a = 3.121192 \times 10^{-13}$, Normal form coefficient = 2.294637×10^{-18}. The cycles that appeared in PD/LPC are similar in size and spatially separated in phase space, possibly due to special conditions in the dynamical system, such as symmetric structure.

In Figure 8, at the LP, two equilibria (one stable-solid curve and one unstable-dashed curve) meet and vanish, indicating a saddle-node bifurcation (or fold bifurcation). The equilibrium points merge and disappear as φ crosses the LP. After this point, no equilibrium points exist in this parameter range. As φ increases, the concentration of DLBCL cells rises, while other cells oscillate slightly but tend to remain constant. After crossing the LP point, φ decreases, but DLBCL cells continue to increase. This suggests that beyond the LP, the growth of DLBCL cells becomes increasingly unchecked, alongside a decrease in the decay rate of immune cells (φ). Overall, the concentration of DLBCL cells appears to correlate positively with the decay rate of effector cells induced by DLBCL cells (φ). In contrast, the concentration of normal cells tends to remain constant. The neutral saddle in Figure 8 reflects a dynamic equilibrium between the concentrations of normal cells and DLBCL cells, where neither significantly increases nor decreases. These conditions still allow for small fluctuations in cell population, without a strong tendency toward convergence or divergence. The immune system attempts to control the growth of DLBCL cells without damaging or eliminating normal cells. While the concentration of DLBCL cells remains steady, further growth is possible without treatment or effective control.

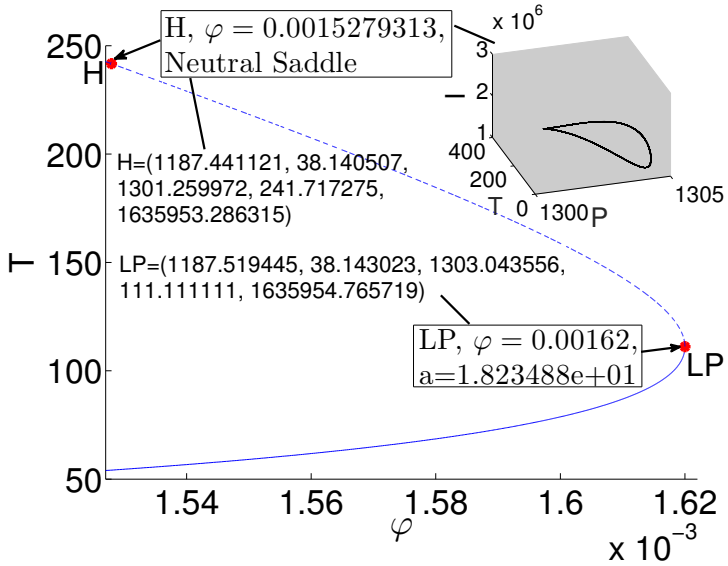

Figure 8. Continuation is performed starting from $\varphi = 3.422 \times 10^{-11}$ with the non-hyperbolic equilibrium E_{5-} as the initial condition in region IV. As φ varies, a bifurcation scenario is revealed, where a non-degenerate limit point (LP) is detected at $\varphi = 0.001620$ with eigenvalues -9.44161, -1.95888, -0.100111, $-6.93749 \times 10^{-8} \pm i3.29047 \times 10^{-6}$, indicating two eigenvalues approaching zero. Additionally, neutral saddle is found at $\varphi = 0.0015279313$ with eigenvalues -9.44161, -1.95875, -0.100242, -0.100242, and 0.100242.

In Figure 7, where a is positive, the occurrence of limit cycles and periodic dynamics can be interpreted as indicating a balanced state, potentially reflecting tumor dormancy. This behavior may correspond to a situation where the DLBCL lymphoma mass maintains a balance between proliferation and decline due to the presence of effector cells [49]. However, Figure 9 presents results for negative values of a, where the dynamics remain purely mathematical, and no direct biological conclusions can be drawn from this analysis. Meanwhile, the dynamics around the Generalized Hopf (GH) point also exhibit oscillations in the system; see Figure 10 (right). However, the biological interpretation of this phenomenon also requires further examination, as the parameters supporting it are not always realistic in a biological context.

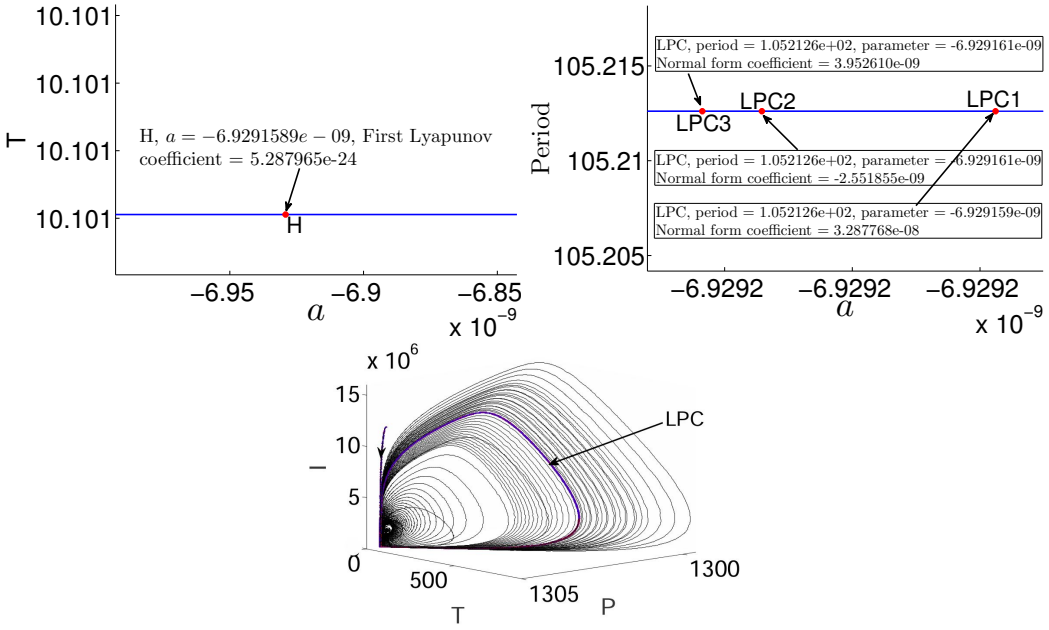

Figure 9. Starting from $a = 2.2 \times 10^{-11}$ with E_{5-} as the initial value in region IV, continuation is performed by varying a. This reveals the emergence of a non-degenerate Hopf bifurcation at $a = -6.929159 \times 10^{-9}$ with $H = (1187.580021, 38.144969, 1304.426164, 10.101010, 1635956.027314)$ (left). The continuation of Hopf's point on the a and its period produces the LPC (right). Additionally, the phase portrait around the Hopf point, considering values of a both less than and greater than -6.929159×10^{-9}, shows oscillations (bottom). The phase portraits for both conditions were displayed on the same graph for comparison, in order to observe the dynamics for $a < -6.929159 \times 10^{-9}$ and $a > -6.929159 \times 10^{-9}$ (bottom). From a biological perspective, the interpretation remains unclear for $a < -6.929159 \times 10^{-9}$. The negative values observed in this continuation are included for completeness and do not impact the biological conclusions of this study. Conversely, as a increases from values just above -6.929159×10^{-9} (negative) to small positive values and eventually larger positive values, the concentration of DLBCL and effector cells decreases, showing small fluctuations. These trends reflect the mathematical structure of the model, and their biological significance, if any, remains unclear.

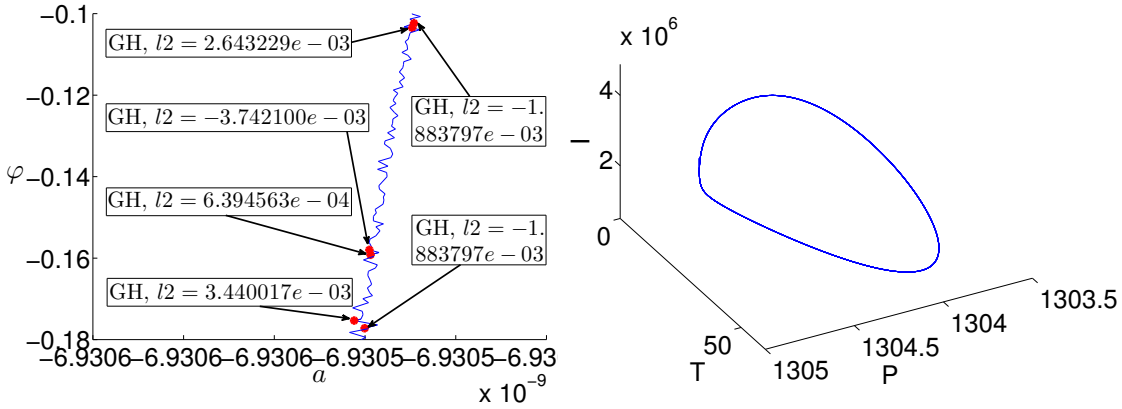

Figure 10. A generalized Hopf (GH) bifurcation curve (left) is obtained by continuing the Hopf point, previously determined (in Figure 9), with respect to the parameters a and φ. The dynamics of the solution that occurs around the GH point is depicted by taking the values $a = -6.930539 \times 10^{-9}$ and $\varphi = -0.15797224$ (right).

Bifurcation analysis of a in region V, as shown in Figure 11, reveals that decreasing a raises the carrying capacity, leading to higher DLBCL concentration. These bifurcation structures highlight that changes in the tumor microenvironment affecting carrying capacity may drive disease progression. Such alterations could serve as early indicators of more aggressive DLBCL behavior.

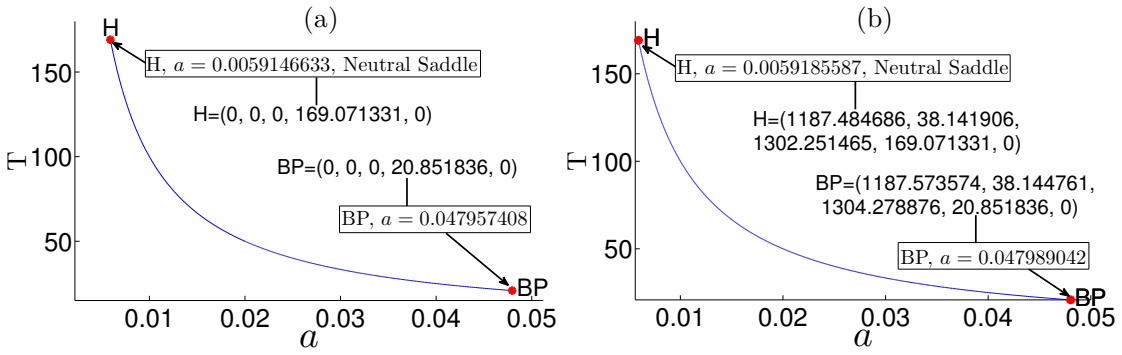

Figure 11. Bifurcation diagram in region V under the variation of a, starting from $a = 2 \times 10^{-2}$: (a) Continuation from the equilibrium $E_2 = (0, 0, 0, 50, 0)$ with respect to a reveals a neutral saddle and a branch point; (b) Continuation from $E_6 = (1187.556074, 38.14419937, 1303.879249, 50.03297117, 0)$ results in a branch point (BP) and a neutral saddle. A decrease in the value of a indicates an increase in the carrying capacity, which in turn leads to an increase in DLBCL concentration, and vice versa.

Figures 12 and 13, respectively, show the trajectories near saddle points E_{4+} and E_{5+} in region VI with $a = 1 \times 10^{-5}$, $\varphi = 1 \times 10^{-4}$, yielding locally asymptotically stable E_6. The concentration of DLBCL has increased, whereas the effector cells reach zero. This condition may be a sign that the immune system is losing its ability to effectively fight the DLBCL growth, which could be linked to progression to a higher stage or malignancy of the DLBCL. Then, by selecting $a = 1 \times 10^{-6}$,

$\varphi = 1.7 \times 10^{-3}$, in region VII we obtain 4 nonnegative points: Three unstable equilibria (E_0, E_1, E_2) and one locally asymptotically stable (E_6).

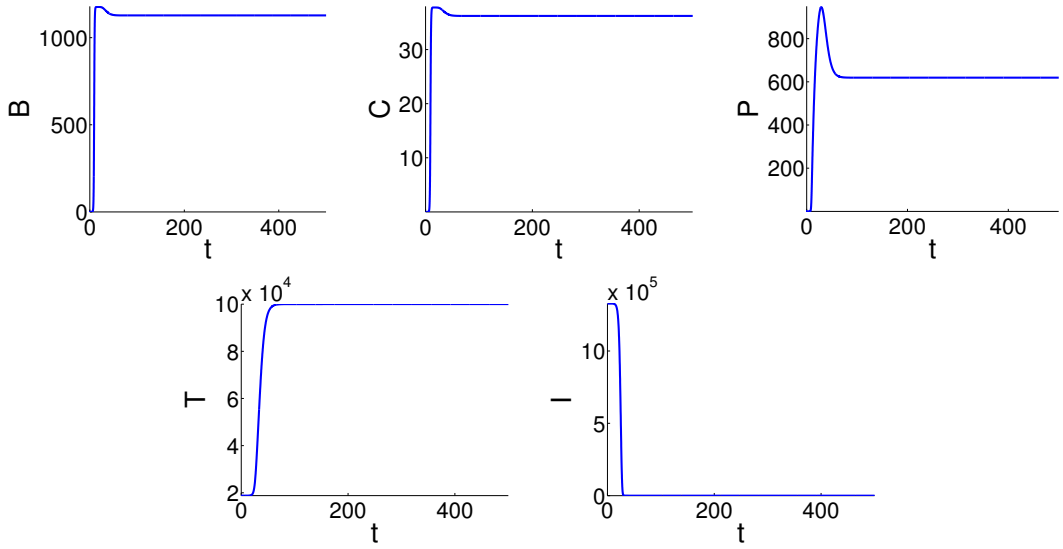

Figure 12. Trajectories near saddle points E_{4+} in region VI with $a = 1 \times 10^{-5}$, $\varphi = 1 \times 10^{-4}$.

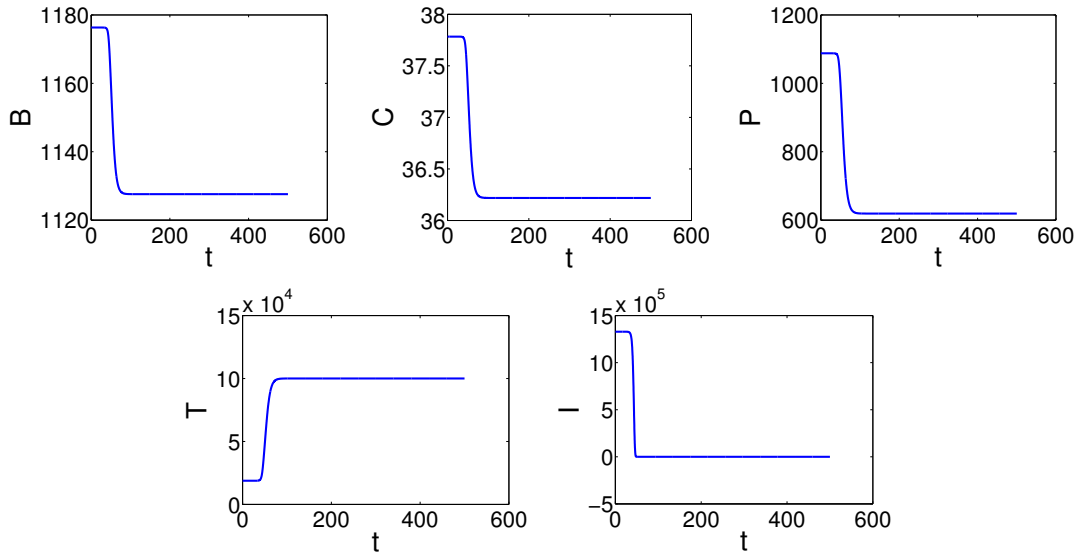

Figure 13. Trajectories near saddle points E_{5+} in region VI with $a = 1 \times 10^{-5}$, $\varphi = 1 \times 10^{-4}$.

Other findings show that the concentration of DLBCL cells remains constant over an extended period, while other cell populations tend to approach zero; see Figure 6. The local asymptotic stability observed in point E_2 provides compelling evidence for this phenomenon. This phenomenon could indicate that DLBCL lymphoma triggers the immune system's "immune evasion" mechanism to evade the body's defenses [50]. Lymphoma cells possess the capability to "hide" from the immune system through the reduction of the expression of molecules crucial for antigen presentation or, in some

cases, their complete elimination. In addition, lymphoma cells can also develop resistance to apoptosis through several chemical pathways, such as the Granzyme pathway. Furthermore, the interaction of lymphoma cells with their microenvironment may favor their escape from the immune system through the formation of an "Immunosuppressive Microenvironment," such as through the cytokine interleukin-10 with an immunosuppressive role.

Efforts to overcome immune evasion in DLBCL are one of the main challenges in therapy because a single therapy or monotherapy may not be effective enough in DLBCL. Insights into the model's phenomena have therapeutic implications that can direct the development of treatments like combination therapies and even "personalized medicine". This aims to increase the effectiveness of treatment to better suit the specific conditions and characteristics of the patient while reducing the treatment side effects. Immune checkpoint inhibition is a form of customized immunotherapy treatment that is effective in lung cancer and hematological malignancies [50], the purpose is to revive the body's immune response to cancer. Thus, understanding the phenomena of the model can provide insight for clinicians in designing treatments that are more precise and personalized to the complexity of the patient.

4. Conclusions

The mathematical model developed in this study offers a novel contribution to understanding diffuse NHL growth, specifically focusing on the interactions between DLBCL cells and the immune system. This model includes important assumptions that simplify complex biological processes into mathematical forms, allowing for quantitative analysis. Through this analysis, several equilibrium points have been identified, providing insights into asymptotically stable conditions where lymphoma growth may either stop or persist. Numerical bifurcations show that the carrying capacity "$1/a$" and the loss rate of effector cells due to DLBCL cell interactions "φ" play a role in controlling the dynamics of the model solution and maintaining the DLBCL concentration constant. There are indications of bifurcation, such as Hopf, limit points, and branch points. We also detect neutral saddle, period doubling, generalized Hopf, and limit point cycles. The chaotic phenomenon that we found indicates that the model used to comprehend the growth characteristics of DLBCL is a system sensitive to initial conditions. This further highlights the complexity of the interactions between DLBCL cells and effectors, as even minor differences in the cellular environment or patient's starting condition can significantly affect the course of the DLBCL progression and the immune response. The discovery of some phenomena also provides valuable insights into how variations in both parameters may influence lymphoma progression, potentially relevant for planning therapeutic strategies.

Although this model offers new contributions, the system's complexity makes it challenging to analyze the stability of all equilibrium points, particularly for highly nonlinear parameters. While numerical approaches have been helpful in bifurcation analysis, the results still depend on the choice of initial parameters, which can affect the generalizability of these findings. Sensitivity analysis aids in selecting the appropriate bifurcation parameters by highlighting those that most significantly impact the model's results. Sensitivity analysis by integrating relevant clinical data to identify the most influential parameters on DLBCL growth dynamics, validate the model, and improve prediction accuracy is one of our future research considerations. Furthermore, an analytical approach is needed to determine the normal form of the bifurcation. The development of more sophisticated analysis methods to explore

the stability and bifurcation of these system is also needed. Additionally, perturbation methods could be used to examine the impact of small parameter variations on system stability.

It is important to realize that mathematical models can provide new insights but cannot always reflect all aspects of clinical field situations because models are generally based on assumptions and limitations. Therapeutic decisions are so complex that it is not enough to simply consider them from the perspective of mathematical models but also based on clinical data and a deep understanding of each patient's unique situation. The current model provides a basic understanding of DLBCL dynamics without medical intervention. Although there are some limitations in this study, one that should be considered is that some parameter values in bifurcation phenomena may not be biologically meaningful, as they can become negative when bifurcation curves extend into certain regions, even though these dynamics remain mathematically significant. Refining parameter constraints will be necessary to ensure biological feasibility while preserving the key dynamical properties of the model. To better simulate lymphoma growth dynamics more realistically and predictively, models should consider variables such as dosage and frequency of therapy. Future studies also may concentrate on the pathways connected to apoptosis resistance, immunosuppression, and the addition of therapeutics as controls, as well as the mechanisms of DLBCL immune evasion. The integration of actual clinical data is essential to validate the results and improve model accuracy. Further research will focus on understanding the characteristics of DLBCL by combining specific clinical data, particularly those related to immune evasion and apoptosis resistance, in collaboration with experimental researchers. This approach is expected to validate the results, improve model accuracy, and provide new perspectives for cancer biologists, thereby accelerating progress in understanding the growth mechanisms of DLBCL.

Author contributions

All authors contributed to the study, including conceptualization, formal analysis, investigation, validation, visualization, and the writing, review, and editing of the manuscript. All authors have read and approved the final version of the manuscript for publication.

Use of Generative-AI tools declaration

The authors declare they have not used Artificial Intelligence (AI) tools in the creation of this article.

Acknowledgments

The authors would like to thank Department of Mathematics, Faculty of Mathematics and Natural Sciences, Universitas Gadjah Mada for the support on this research. This work is partially funded by Universitas Gadjah Mada through the research scheme "Rekognisi Tugas Akhir" 2023 with the letter of assignment number 5075/UN1.P.II/Dit-Lit/PT.01.01/2023.

Conflicts of interest

The authors declare that they have no conflicts of interest.

References

1. F. Bray, M. Laversanne, H. Sung, J. Ferlay, R. L. Siegel, I. Soerjomataram, et al., Global cancer statistics 2022: GLOBOCAN estimates of incidence and mortality worldwide for 36 cancers in 185 countries, *CA: A Cancer Journal for Clinicians*, **74** (2024), 229–263. https://doi.org/10.3322/caac.21834
2. *Lymphoma*, Cancer Australia, 2022. Available from: `https://www.canceraustralia.gov.au/cancer-types/lymphoma/overview`
3. R. L. Siegel, K. D. Miller, N. S. Wagle, A. Jemal, Cancer statistics, 2023, *CA: A Cancer Journal for Clinicians*, **73** (2023), 17–48. https://doi.org/10.3322/caac.21763
4. N. Anggorowati, Indrawati, A. L. Dhyanti, H. Arkananda, S. H. Rizki, S. A. Setiawan, et al., Sociodemographic and Clinicopathological features of Lymphoma patients in Indonesia: A report from special region of Yogyakarta province, *Asian Pacific J. Envir. Canc.*, **4** (2022), 33–38. https://doi.org/10.31557/apjec.2021.4.1.33-38
5. A. A. Alizadeh, M. B. Eisen, R. E. Davis, C. Ma, I. S. Lossos, A. Rosenwald, et al., Distinct types of diffuse large B-cell lymphoma identified by gene expression profiling, *Nature,* **403** (2000), 503–511. https://doi.org/10.1038/35000501
6. A. Rosenwald, G. Wright, K. Leroy, X. Yu, P. Gaulard, R. D. Gascoyne, et al., Molecular diagnosis of primary mediastinal B cell lymphoma identifies a clinically favorable subgroup of diffuse large B cell lymphoma related to Hodgkin lymphoma, *J. Exp. Med.*, **198** (2003), 851–862. https://doi.org/10.1084/jem.20031074
7. Y. Liu, S. K. Barta, Diffuse large B-cell lymphoma: 2019 update on diagnosis, risk stratification, and treatment, *Am. J. Hematol.*, **94** (2019), 604–616. https://doi.org/10.1002/ajh.25460
8. The International Non-Hodgkin's Lymphoma Prognostic Factors Project, A predictive model For aggressive Non-Hodgkin's Lymphoma, *The New England J. Medic.*, **329** (1993), 987–994. https://doi.org/10.1056/NEJM199309303291402
9. L. H. Sehn, B. Berry, M. Chhanabhai, C. Fitzgerald, K. Gill, P. Hoskins. et al., The revised International Prognostic Index (R-IPI) is a better predictor of outcome than the standard IPI for patients with diffuse large B-cell lymphoma treated with R-CHOP, *Blood*, **109** (2007), 1857–1861. https://doi.org/10.1182/blood-2006-08-038257
10. Z. Zhou, L. H. Sehn, A. W. Rademaker, L. I. Gordon, A. S. Lacasce, A. Crosby-Thompson, et al., An enhanced international prognostic index (NCCN-IPI) for patients with diffuse large B-cell lymphoma treated in the rituximab era, *Blood*, **123** (2014), 837–842. https://doi.org/10.1182/blood-2013-09-524108
11. H. M. Byrne, Dissecting cancer through mathematics: From the cell to the animal model, *Nat. Rev. Cancer*, **10** (2010), 221–230. https://doi.org/10.1038/nrc2808
12. L. G. de Pillis, A. Radunskaya, A mathematical tumour model with immune resistance and drug therapy: An optimal control approach, *J. Theor. Med.*, **3** (2001), 79–100. https://doi.org/10.1080/10273660108833067

13. L. G. de Pillis, A. Radunskaya, A mathematical model of immune response to tumor invasion, *Comput. Flu. Solid Mecha.*, **2003** (2003), 1661–1668. https://doi.org/10.1016/B978-008044046-0.50404-8

14. T. S. N. Asih , S. Lenhart, S. Wise, L. Aryati, F. Adi-Kusumo, M. S. Hardianti, et al., The dynamics of HPV infection and cervical cancer cells, *Bull. Math. Biol.*, **78** (2016), 4–20. https://doi.org/10.1007/s11538-015-0124-2

15. F. Adi-Kusumo, R. S. Winanda, Bifurcation analysis of the cervical cancer cells, effector cells, and IL-2 compounds interaction model with immunotherapy, *Far East J. Math.l Sci.*, **99** (2016), 869–883. https://doi.org/10.17654/MS099060869

16. S. Suddin, F. Adi-Kusumo, L. Aryati, Gunardi, Reaction-diffusion on a spatial mathematical model of cancer immunotherapy with effector cells and IL-2 compounds' interactions, *Int. J. Differ. Equ.*, **2021** (2021), 5535447. https://doi.org/10.1155/2021/5535447

17. E. R. Sari, L. Aryati, F. Adi-Kusumo, An age-structured SIPC model of cervical cancer with immunotherapy, *AIMS Math.*, **9** (2024), 14075–14105. https://doi.org/10.3934/math.2024685

18. J. Malinzi, R. Ouifki, A. Eladdadi, D. F. M. Torres, K. A. J. White, Enhancement of chemotherapy using oncolytic virotherapy: Mathematical and optimal control analysis, *Math. Biosci. Eng.*, **15** (2018), 1435–1463. https://doi.org/10.3934/mbe.2018066

19. F. Adi-Kusumo, L. Aryati, S. Risdayati, S. Norhidayah, Hopf bifurcation on a cancer therapy model by oncolytic virus involving the malignancy effect and therapeutic efficacy, *Int. J. Math. Math. Sci.*, **2020** (2020). https://doi.org/10.1155/2020/4730715

20. S. S. Balasubramaniam, H. M. Safuan, F. Adi-Kusumo, On the bifurcation of a cancer therapy model by oncolytic virus with malignancy effect, *EKST*, **4** (2024), 1–10.

21. M. I. A. Fathoni, Gunardi, F. Adi-Kusumo, S. H. Hutajulu, Mathematical model analysis of breast cancer stages with side effects on heart in chemotherapy patients, *AIP Conf. Proc.*, **2192** (2019), 060007. https://doi.org/10.1063/1.5139153

22. M. I. A. Fathoni, F. Adi-Kusumo, Gunardi, S. H. Hutajulu, Dynamics of a breast cancer model for neutropenia case due to chemotherapy effects, *Int. J. Differ. Equ.*, **2021** (2021), 1–8. https://doi.org/10.1155/2021/3401639

23. M. I. A. Fathoni, F. Adi-Kusumo, Gunardi, S. H. Hutajulu, Mathematical model of the journey of breast cancer patients affected by chemotherapy response, *Int. J. Differ. Equ.*, **17** (2022), 19–32.

24. W.-L. Duan, H. Fang, C. H. Zeng, The stability analysis of tumor-immune responses to chemotherapy system with gaussian white noises, *Chaos Soliton. Fract.*, **127** (2019), 96–102. https://doi.org/10.1016/j.chaos.2019.06.030

25. W. L. Duan, The stability analysis of tumor-immune responses to chemotherapy system driven by Gaussian colored noises, *Chaos Soliton. Fract.*, **141** (2020). https://doi.org/10.1016/j.chaos.2020.110303

26. T. Alarcón, R. Marches, K. M. Page, Mathematical models of the fate of lymphoma B cells after antigen receptor ligation with specific antibodies, *J. Theor. Biol.*, **240** (2006), 54–71. https://doi.org/10.1016/j.jtbi.2005.08.028

27. K. Roesch, D. Hasenclever, M. Scholz, Modelling lymphoma therapy and outcome, *Bull. Math. Biol.*, **76** (2014), 401–430. https://doi.org/10.1007/s11538-013-9925-3

28. J. M. Chrobak, M. Bodnar, H. Herrero, About a generalized model of lymphoma, *J. Math. Anal. Appl.*, **386** (2012), 813–829. https://doi.org/10.1016/j.jmaa.2011.08.043

29. S. Sabir, O. León-Triana, S. Serrano, R. Barrio, V. M. Pérez-G, Mathematical model of CAR T-cell therapy for a B-Cell lymphoma lymph node, *Bull. Math. Biol.*, **87** (2025), 1–33. https://doi.org/10.1007/s11538-025-01417-1

30. S. R. Ganesh, C. M. Roth, B. Parekkadan, Simulating interclonal interactions in diffuse large B-Cell lymphoma, *Bioengineering*, **10** (2023), 1–19. https://doi.org/10.3390/bioengineering10121360

31. J. R. Cerhan, A. Kricker, O. Paltiel, C. R. Flowers, S. S. Wang, A. Monnereau, et al., Medical history, lifestyle, family history, and occupational risk factors for diffuse large B-cell lymphoma: The InterLymph Non-Hodgkin Lymphoma subtypes project, *JNCI Monographs*, **2014** (2014), 15–25. https://doi.org/10.1093/jncimonographs/lgu010

32. M. Muramatsu, K. Kinoshita, S. Fagarasan, S. Yamada, Y. Shinkai, T. Honjo, Class switch recombination and hypermutation require activation-induced cytidine deaminase (AID), a potential RNA editing enzyme, *Cell*, **102** (2000), 553–563. https://doi.org/10.1016/s0092-8674(00)00078-7

33. K. Basso, R. Dalla-Favera, Germinal centres and B cell lymphomagenesis, *Nat. Rev. Immunol.*, **15** (2015), 172–184. https://doi.org/10.1038/nri3814

34. C. Mlynarczyk, L. Fontán, A. Melnick, Germinal center-derived lymphomas: The darkest side of humoral immunity, *Immunol. Rev.*, **288** (2019), 214–239. https://doi.org/10.1111/imr.12755

35. L. Pasqualucci, Molecular pathogenesis of germinal center-derived B cell lymphomas, *Immunol. Rev.*, **288** (2019), 240–261. https://doi.org/10.1111/imr.12745

36. L. Khodadadi, Q. Y. Cheng, A. Radbruch, F. Hiepe, The maintenance of memory plasma cells, *Front. Immunol.*, **10** (2019), 1–17. https://doi.org/10.3389/fimmu.2019.00721

37. D. Kirschner, J. C. Panetta, Modeling immunotherapy of the tumor-immune interaction, *J. Math. Biol.*, **37** (1998), 235–252. https://doi.org/10.1007/s002850050127

38. M. Oprea, A. S. Perelson, Somatic mutation leads to efficient affinity maturation when centrocytes recycle back to centroblasts, *J. Imunol.*, **158** (1997), 5155–5162. https://doi.org/10.4049/jimmunol.158.11.5155

39. V. A. Kuznetsov, I. A. Makalkin, M. A. Taylor, A. S. Perelson, Nonlinear dynamics of immunogenic tumors: Parameter estimation and global bifurcation analysis, *Bull. Math. Biology*, **56** (1994), 295–321. https://doi.org/10.1007/BF02460644

40. Y. B. Jia, Roots of polynomials, *Com S 477/577 Notes*, 2017.

41. N. Suefuji, D. Niino, F. Arakawa, K. Karube, Y. Kimura, J. Kiyasu, et al., Clinicopathological analysis of a composite lymphoma containing both T- and B-cell lymphomas, *Pathol. Inter.*, **62** (2012), 690–698. https://doi.org/10.1111/j.1440-1827.2012.02858.x

42. A. Dhooge, W. Govaerts, Y. A. Kuznetsov, MATCONT: A MATLAB package for numerical bifurcation analysis of ODEs, *ACM T. Mathe. Software*, **29** (2003), 21–22. https://doi.org/10.1145/980175.980184

43. T. D. Chan, D. Gatto, K. Wood, T. Camidge, A. Basten, R. Brink, Antigen affinity controls rapid T-dependent antibody production by driving the expansion rather than the differentiation or extrafollicular migration of early plasmablasts, *J. Immunol.*, **183** (2009), 3139–3149. https://doi.org/10.4049/jimmunol.0901690

44. L. G. de Pillis, A. E. Radunskaya, C. L. Wiseman, A validated mathematical model of cell-mediated immune response to tumor growth, *Cancer Res.*, **65** (2005), 7950–7958. https://doi.org/10.1158/0008-5472.CAN-05-0564

45. P. Calabrese, D. Shibata, A simple algebraic cancer equation: Calculating how cancers may arise with normal mutation rates, *BMC Cancer*, **10** (2010). https://doi.org/10.1186/1471-2407-10-3

46. S. H. Kleinstein, J. P. Singh, Toward quantitative simulation of germinal center dynamics: Biological and modeling insights from experimental validation, *J. Theor. Biol.*, **211** (2001), 253–275. https://doi.org/10.1006/jtbi.2001.2344

47. M. Meyer-Hermann, A. Deutsch, M. Or-Guil, Recycling probability and dynamical properties of germinal center reactions, *J. Theor. Biol.*, **210** (2001), 265–285. https://doi.org/10.1006/jtbi.2001.2297

48. M. E. Meyer-Hermann, P. K. Maini, D. Iber, An analysis of B cell selection mechanisms in germinal centers, *Math. Med. Biol.*, **23** (2006), 255–277. https://doi.org/10.1093/imammb/dql012

49. H. Endo, M. Inoue, Dormancy in cancer, *Cancer Sci.*, **110** (2018), 474–480. https://doi.org/10.1111/cas.13917

50. M. de Charette, R. Houot, Hide or defend, the two strategies of lymphoma immune evasion: Potential implications for immunotherapy, *Haematologica*, **103** (2018), 1256–1268. https://doi.org/10.3324/haematol.2017.184192

Appendix A

In this section, we provide the detailed derivation of the existence and stability conditions for equilibrium points E_4 and E_4, which define the bifurcation boundaries illustrated in Figure 3. The existence condition for E_4 determines the bifurcation boundary, which is given by the following:

$$0 < \frac{1}{2}\frac{1.98 - 1000\varphi \pm \sqrt{(1.98 - 1000\varphi)^2 - 80\varphi}}{\varphi} < \frac{1}{a}.$$

Similarly, the stability conditions for E_4 define additional constraints, given by:

$$\begin{aligned}
&1.980299786 \times 10^6 < \frac{1}{2}\frac{1.98 - 1000\varphi - \sqrt{(1.98 - 1000\varphi)^2 - 80\varphi}}{\varphi},\\
&-1 \times 10^5 < \frac{1}{2}\frac{1.98 - 1000\varphi - \sqrt{(1.98 - 1000\varphi)^2 - 80\varphi}}{\varphi},\\
&(1.98 - 1000\varphi)^2 > 80\varphi.
\end{aligned}$$

For equilibrium E_5, its existence conditions also determine a bifurcation boundary, expressed as:

$$0 < \frac{1}{2}\frac{(1.98 - 1000 \times \varphi \pm \sqrt{(1.98 - 1000\varphi)^2 - 80.00\varphi}}{\varphi} < 1.980299786 \times 10^6,$$

$$-1 \times 10^5 < \frac{1}{2}\frac{1.98 - 1000\varphi \pm \sqrt{(1.98 - 1000\varphi)^2 - 80\varphi}}{\varphi} < \frac{1}{a}.$$